POTENTIAL TRADE-OFFS BETWEEN BIOMINERALIZATION AND IMMUNITY REVEALED BY SHELL PROPERTIES AND GENE EXPRESSION PROFILES OF TWO CLOSELY RELATED *CRASSOSTREA* SPECIES

Anna V. Ivanina[1†], Ballav M. Borah[2†], Angela Vogts[3], Ifra Malik[4], Jingyao Wu[5], Adam R. Chin[5]; Alejandro J. Almarza[2,5], Prashant Kumta[5], Helen Piontkivska[6], Elia Beniash[2,5]*, and Inna M. Sokolova[7]*

[1]Department of Biological Sciences, University of North Carolina at Charlotte, Charlotte, NC, USA

[2]Department of Oral Biology, School of Dental Medicine, University of Pittsburg, Pittsburg, PA, USA

[3]Leibniz Institute for Baltic Sea Research Warnemünde, Warnemünde, Germany.

[4]Dietrich School of Arts and Sciences, University of Pittsburgh, Pittsburgh, PA,, USA

[5]Department of Bioengineering, Swanson School of Engineering, University of Pittsburgh, Pittsburgh, PA, USA

[6]Department of Biological Sciences, Kent State University, Kent, OH, USA

[7]Department of Marine Biology, Institute of Biosciences, University of Rostock, Rostock, Germany

† Equal contributions

***Corresponding authors:** Inna Sokolova Inna.Sokolova@uni-rostock.de; Elia Beniash ebeniash@pitt.edu

Keywords: Gene transcription, matrix proteins, biomineralization, immunity, shell mechanical properties, intracellular mineral transport, hemocytes, mantle, bivalves

Abstract

Species of Ostreidae family are key ecosystem engineers and many of them (including *Crassostrea gigas* and *C. virginica*) are commercially important aquaculture species. Despite similarities in their morphology and ecology, these two species differ in their ability to defend against pathogens potentially reflecting species-specific differential specialization of hemocytes on immune defense vs. biomineralization. To test this hypothesis, we investigated the expression levels of immune and biomineralization-related genes as well as mineralogical and mechanical properties of the shells and the calcium sequestration ability of the hemocytes of *C. gigas* and *C. virginica*. The expression of biomineralization related genes was higher in *C. virginica* than in *C. gigas* in multiple tissues including mantle edge and hemocytes, while the expression of immune genes was higher in the hemocytes of *C. gigas*. Hemocytes of *C. virginica* contained more calcium (stored intracellularly as calcium carbonate mineral) compared with those of *C. gigas*. Analysis of the adult shells showed that the crystallinity of calcite was higher and the laths of the foliated layer of the shell were thicker in *C. virginica* than in *C. gigas*. Mechanically the shells of C. virginica were stiffer, harder and stronger than those of *C. gigas*. Taken together, our results show that the species-specific differences in physiology (such as disease resistance and exoskeleton properties) are reflected at the cellular and molecular levels in differential specialization of hemocytes on potentially competing functions (immunity and biomineralization) as well as different expression profiles of other tissues involved in biomineralization (such as the mantle edge).

List of symbols and abbreviations

ASW	artificial seawater
CA	carbonic anhydrase
CK	casein kinase
CS	chitin synthase
Cq3	complement component 3
DMSO	dimethyl sulfoxide
ECM	extracellular matrix
EDTA	ethylenediaminetetraacetic acid
FTIR	Fourier-transform infrared spectroscopy
HC	hemocyte
HEPES	2-[4-(2-hydroxyethyl)piperazin-1-yl]ethanesulfonic acid
HR SEM	high-resolution scanning electron microscopy
ICP-MS	inductively coupled plasma mass spectrometry
LP	long pass
NanoSIMS	nanoscale secondary ion mass spectrometry
NHE3	Na^+/H^+ antiporter 3
NHX9	Na^+/H^+ antiporter 9
OME	outer mantle edge
PCA	principal component analysis
PM Ca ATPase	plasma membrane Ca^{2+} ATPase
qRT-PCR	quantitative real-time PCR
SEM	standard error of the mean
SLP	silk-like protein
SAED	selected area elector diffraction
SRCR	scavenger receptor cysteine rich
TLR	toll-like receptor
TNF	tumor necrosis factor
VEGF	vascular endothelial growth factor
VEGF-R	vascular endothelial growth factor receptor

Estuaries and coastal zones are areas of high productivity characterized by high degree of abiotic stress. Many oyster species, including the Pacific oyster *Crassostrea gigas* and the Eastern oyster *Crassostrea virginica*, are ecosystem engineers in estuarine and coastal habitats and economically important species supporting multimillion fisheries and aquaculture worldwide (FAO, 2017). Like many benthic sessile species, oysters have limited ability to escape environmental stressors or predators and rely on mechanical protection (provided by shells) (Kocot et al., 2016) and physiological and biochemical adjustments (Sokolova et al., 2011) to survive predator attacks and/or shifts in the environmental conditions. Furthermore, due to their filter-feeding habit, oysters are exposed to large amounts and diversity of parasites and pathogens, with an average oyster encountering tens to hundreds thousands of microbes per second (Allam and Pales Espinosa, 2016; Ben-Horin et al., 2015). In past decades, oyster diseases have expanded in range and increased in severity often causing staggering losses in the impacted species (Barbosa Solomieu et al., 2015; Beck et al., 2011; Ford and Smolowitz, 2007; Ford, 1996). These conditions put high selective pressure on the protective mechanisms against abiotic and biotic stressors for oyster survival. While oysters are ecologically dominant species in many estuaries, there is considerable variation in the tolerance to disease and environmental stressors between closely related species of oysters. Thus, the Pacific (*C. gigas*) and Eastern (*C. virginica*) oysters have similar ecology and feeding habits, yet display a stark difference in disease resistance (Barbosa Solomieu et al., 2015; Elston, 1993; Salvi et al., 2014). The Pacific oyster *C. gigas* is disease tolerant and rarely suffers epizootics despite serving as a host to a variety of bacteria, viruses and eukaryotic parasites (Barbosa Solomieu et al., 2015; Chu et al., 1996; Elston, 1993). In contrast, *C. virginica* commonly experience mass mortalities due to epizootics caused by unicellular eukaryotic parasites *Haplosporidium nelsoni* and *Perkinsus marinus* as well as bacterial and viral agents (Barbosa Solomieu et al., 2015; Elston, 1993; Ford, 1996). These remarkable species-specific differences in disease susceptibility between *C. gigas* and *C. virginica* have been linked to the differences in immunocompetence (Guo et al., 2015). Thus, *C. gigas* immune cells can better avoid the subversion of the immune defense by the parasite and are more capable of the parasite destruction compared to *C. virginica* hemocytes (Foster et al., 2011; Goedken et al., 2005; Hughes et al., 2010; Sunila and LaBanca, 2003). Hemolymph of *C. gigas* also contains higher levels of protease inhibitors that prevent cell lysis by a eukaryotic parasite *Perkinus marinus* compared with the hemolymph of *C. virginica* (MacIntyre et al., 2003; Romestand et al., 2002). These data show that the interspecific differences in cell-based and humoral immunity may contribute to the differences in the disease susceptibility between the Pacific and Eastern oysters. However, the molecular mechanisms underlying these differences are not yet fully understood.

Hemocytes are multifunctional cells that play a key role in innate immune defense, wound repair and biomineralization of oysters (Wang et al., 2018). Oyster hemocytes are involved in recognition, opsonization and destruction of the pathogens through phagocytosis,

oxidative burst and production of a wide range of antimicrobial compounds (Arumugan et al., 2000; Defer et al., 2013; Gourdon et al., 2001; Hellio et al., 2007). They recognize and encapsulate the foreign bodies and participate in wound repair (Ford, 1996; Perez and Fontanetti, 2010). Recent studies have also demonstrated a key role of hemocytes in biomineralization due to their involvement in the mineral transport, as well as production of the extracellular matrix (ECM) of the shells (Ivanina et al., 2017; Johnstone et al., 2015; Li et al., 2016; Mount et al., 2004). Notably, different populations of hemocytes of *C. gigas* (separated by the different floating density) are mostly specialized on either immune defense or biomineralization (Ivanina et al., 2017; Wang et al., 2017b). The developmental mechanisms and physiological consequences of the functional diversity of oyster hemocytes are not yet fully understood, and it remains unclear whether different types of hemocytes represent true differentiated subpopulations, different developmental stages or functional plasticity (Rebelo et al., 2013; Wang et al., 2017b). Regardless of the mechanisms of the functional differentiation, specialization on either immune defense or biomineralization might imply a potential trade-off between these two functions of hemocytes.

The aim of the present study was to investigate the potential interspecific differences in hemocyte involvement in immune defense and biomineralization in two closely related oyster species, *C. gigas* and *C. virginica.* We hypothesized that the species-specific differences in the shell properties and disease resistance of oysters are reflected in the prevailing specialization of their hemocytes on either biomineralization or immune defense. To test this hypothesis, we assessed expression of the key biomineralization genes (including genes involved in ion regulation, Ca^{2+} transport, cell-cell interactions and ECM formation) in two main biomineralizing tissues (the hemocytes and the mantle) and assessed the microstructure and mechanical properties of the shells of *C. gigas* and *C. virginica*. We also determined mRNA expression of immune defense genes (including molecular pattern-recognition genes as well as humoral and inflammation-related factors) and the capacity for phagocytosis and mineral transport in the hemocytes of these two congeners. This study provides important insights into the relative immunocompetence and capacity for biomineralization of hemocytes of two ecologically and economically important *Crassostrea* species that may have implications for mechanistic understanding of the species-specific differences in shell properties, mechanical protection and the ability to deal with pathogens.

MATERIALS AND METHODS

Animal collection and maintenance. Oysters *C. gigas* (Thunberg, 1793) (from Fanny Bay, Canada) and *C. virginica* Gmelin, 1791 (from Delaware Bay, NJ, USA) were purchased from a local supplier (Inland Seafood, Charlotte, NC, USA). Oysters were kept in tanks with the artificial seawater (ASW) (Instant Ocean®, Kent Marine, Acworth) at 10±1°C and salinity 30±1 practical salinity units (PSU). They were fed *ad libitum* with a commercial algal blend containing *Nannochloropsis oculata, Phaeodactylum tricornutum* and *Chlorell*a spp. (DT's

Live Marine Phytoplankton, Sycamore, IL, USA). Algal blend (2-3 ml per 20-25 animals) was added to experimental tanks every other day.

Hemolymph and tissue collection. Hemolymph was extracted from the adductor muscle of oysters using sterile 10 ml syringe with a 21 gauge needle containing 1 ml of ice-cold salinity 30 ASW (for functional hemocyte analyses, gene expression studies and NanoSIMS analyses of hemocytes), or 1 ml of ice-cold Alsever's solution containing 20.8 g l^{-1} glucose, 8 g l^{-1} sodium citrate, 3.36 g l^{-1} EDTA, 22.3 g l^{-1} NaCl (for mineralological analyses) to prevent aggregation of the hemocytes. For hemocyte functional analyses and mRNA expression, hemolymph was collected from individual oysters. Soft tissues (the gills, the central part of the mantle and the outer mantle edge) were collected from the same oysters. For FTIR spectroscopy and ICP-MS, hemolymph from 7-10 oysters was pooled to obtain sufficient amount of hemocytes. Hemocytes were enumerated using a Brightline hemocytometer and collected by centrifugation for 10 min at 1000 x g. For functional studies (phagocytosis and adhesion capacity) hemocytes were analyzed immediately; for all other analyses, hemocytes and soft tissue samples were snap-frozen in liquid nitrogen and stored at -80°C until further analysis.

For the analysis of Ca and Mg content, subpopulations of hemocytes were separated by the floating density on discontinuous Percoll density gradient as described elsewhere (Ivanina et al., 2017). Briefly, isolated hemocytes from 7-15 oysters were resuspended in 4 ml of ice-cold Alsever's solution, layered on a discontinuous Percoll gradient (9.2%, 24.8%, 41.0%, 57.8% v/v in Alsever's solution) and centrifuged at 550 x g and +4°C for 40 min. Hemocytes concentrated at the interfaces of the adjacent gradient steps and at the bottom of the tube were collected and labeled H1, H2, H3 and H4 (from top to bottom), respectively. The suspensions containing separate hemocyte subpopulations were diluted 10-12-fold with Alsever's solution and centrifuged at 1000 x *g* for 10 min to eliminate Percoll and collect the cells. The pellets were resuspended in Alsever's solution, snap-frozen in liquid nitrogen and stored at -80°C.

Phagocytosis. Phagocytosis assay was performed as described elsewhere (Ivanina et al., 2014). Briefly, suspension of Neutral Red-stained, heat-stabilized zymozan (Sigma-Aldrich, St. Louis, MO, USA) was added to hemocytes at the final concentration of 200 zymozan particles per hemocyte. Hemocytes were incubated for 30 min at room temperature, centrifuged at 1000 x g for 10 min and washed with ASW (salinity 30) to remove extracellular zymozan. Cell-free suspensions of zymozan were used as calibration standards. HCs or zymozan standards were incubated for 5 min with 1% acetic acid in 50% ethanol to extract the Neutral Red and quantified at 550 nm on a microplate spectrophotometer (Multiscan GO, Thermo Scientific, Waltham, MA, USA). Results are expressed as the number of ingested zymozan particles per 100 cells.

Adhesion capacity. Isolated HCs (5 x 10^5 cells) were placed in 1 ml of ASW (salinity 30) in the wells of a 12-well plate (Costar, Costar, Corning, NY, USA) and incubated for 2 h at room temperature as described elsewhere (Ivanina et al., 2014). After the incubation, the ASW was collected, the wells were surface-washed with 1 ml of ASW, and the ASW from the incubation and the wash was pooled for each well. The samples were centrifuged for 10 min 1000 x g to collect non-adhered cells. The cells were counted using a Brighline hemocytometer, and the adhesion capacity expressed as the percentage of adhered HCs in each sample.

Quantitative real-time PCR (qRT-PCR). Total RNA was extracted from HCs using ZR RNA MiniPrep™ kit (Zymo Research, Irvine, CA, USA) according to the manufacturers' instructions. Total RNA from the central part of the mantle, outer mantle edge and the gills were isolated using TRI Reagent (Sigma-Aldrich, St Louis, MO, USA) according to the manufacturer's instructions. RNA concentration was measured using NanoDrop 2000 spectrophotometer (Thermo Scientific, Pittsburg, USA). Single-stranded cDNA was obtained from 0.2 µg of the total RNA using 50 U μl^{-1} SMARTScribe™ reverse Transcriptase (Clontech, Mountain View, CA, USA) and 20 µmol l^{-1} of oligo$(dT)_{18}$ primers. Transcript expression of target genes was determined by qRT-PCR using a 7500 Fast Real-Time PCR System (Applied BioSystems/Life Technologies, Carlsbad, CA, USA) and SYBR® Green PCR kit (Life Technologies, Bedford, MA, USA) using gene-specific primers (Supplementary Table 1). The qRT-PCR reaction mixture consisted of 7.5 µl of 2 x SYBR® Green master mix, 0.3 µmol l^{-1} of each forward and reverse primers, 1.5 µl of 10 x diluted cDNA template and water to adjust to 15 µl. The reaction mixture was subjected to the following cycling: 10 min at 95°C to denature DNA and activate Taq polymerase and 40 cycles of 15 s at 94°C, 30 s at 60°C and 30 s at 72°C. Serial dilutions of a cDNA standard were amplified in each run to determine apparent amplification efficiency and run-to-run amplification variability (Pfaffl, 2001). The target gene mRNA expression was standardized relative to β-actin mRNA (Sanni et al., 2008).

Inductively coupled plasma mass spectrometry (ICP-MS). Total hemocytes population and density-segregated hemocyte subpopulations H1, H2, H3 and H4 were used in these studies. Prior to the processing, the cell density in each sample was determined using the cell counter slide centrifuged (550×*g*, 40 min, 4°C) and digested in 35% HNO_3 for 24 h at 65° C. The samples were diluted with distilled de-ionized water to achieve the final acid concentration of 3.5% HNO_3 and filtered through 0.20 µm MINISART PLUS membrane filters. The concentrations of calcium were analyzed using ICP-MS spectrometer (Thermo iCAP 6000 Series, Cambridge, UK) and expressed in nmole per cell. Five measurements obtained from the same sample were averaged and used as one biological replicate and three replicates were used for each hemocyte fraction.

Nanoscale secondary ion mass spectrometry (NanoSIMS) analyses. Hemocytes from two oysters were pooled, collected by centrifugation and resuspended in 1 ml ASW (salinity 30). Hemocyte suspension (100 µl) was plated on indium-tin-oxide coated glass slides (Praezisions Glas & Optik GmbH, Iserlohn, Germany) and incubated for 1 h at the room temperature in a humid chamber to permit hemocyte attachment. After 1 h, the slide briefly washed in ultra-pure water to remove salts, fixed for 10 min in 70% ethanol, dehydrated by sequential incubations in 95 and 100% ethanol and air-dried for NanoSIMS analysis. For each species, three biological replicates (each consisting of the pooled hemocytes of two individuals) were analyzed. Two additional biological replicates of *C. gigas* were found to be on slides without sufficient conductibility. They were therefore sputtered with gold by a sputter coater (Cressigton 108auto) and reanalysed. SIMS imaging was performed using a NanoSIMS 50L instrument (Cameca, France). Three individual frames were analyzed for each biological replicate.

The Cs-source of the NanoSIMS instrument was used to erode and ionize atoms of the sample. Among the received secondary ions, images of 12C-, 16O-, 12C14N- and secondary electrons were recorded simultaneously for areas with sufficient cell density. Prior to the analysis, sample areas of 50×50 µm were sputtered for 90 s with 600 pA to reach the steady state of secondary ion formation and clean the surface. The primary ion beam current during the analysis was 1 pA; the scanning parameters were 512×512 pixels for areas of 47x47 µm, with a dwell time of 250 µs per pixel. 60 planes were analyzed. Slightly smaller areas (28 to 35 µm) of the same locations were then analyzed with the NanoSIMS Oxygen-source (Duoplasmatron) and 23Na+, 24Mg+ and 40Ca+ ions were recorded. It is worth noting that SIMS analyses are destructive; therefore, the sequential analyses with the Cs- and the O-source deliver signals from different sample depths, which might biases the Cs/O correlations. However, the sample erosion by the Cs source was shown to be small enough to resolve cell size features (5.7 nm for a similar primary Cs beam in a smaller area; Saka et al., 2014). The primary ion beam current during the analysis was 25 pA; the scanning parameters were 512×512 pixels with a dwell time of 250 µs per pixel. 60 planes were analyzed. Secondary Ions were detected using mass detectors equipped with electron multipliers (Hamamatsu). The instrument was adjusted to reach a mass resolving power appropriate to suppress interferences at all masses allowing the separation of 12C14N- from interfering ions such as 12C21H2-.

NanoSIMS data were analyzed employing the Look@NanoSIMS software (Polerecky et al., 2012). Depending on the signal quality, 58-60 planes were drift corrected and accumulated. The cells were defined as regions of interest (ROIs) employing the Na+ signal and verified by comparison with the CN- and secondary electron pictures. For the gold-coated samples, the accumulated O- and Na+ were used to align the two measurements. To avoid potential bias due to the differences in the analytical procedure, the gold-coated samples were

excluded from the quantitative analyses of the ion ratios. For all other samples, Ca/Mg, Ca/Na and Mg/Na ratios were calculated for each ROI representing individual cells. Cell sizes were calculated from the number of pixels in the ROI assuming elliptical cell shape. Ca/Na and Mg/Na ratios were used as proxies for the relative Ca and Mg concentrations in the hemocytes, assuming that Na density per unit cell area is similar in the osmoconforming mollusks maintained under the same salinity conditions.

Thermogravimetric analysis (TGA). Thermal characteristics of samples were measured with a TGA Q500 thermal analysis system (TA Instruments, New Castle, DE, USA). About 10 mg of powdered dry oyster shell was used for each test. All TGA experiments were performed under nitrogen atmosphere (Balance gas: N_2 purge rate 40.0 ml/min; Sample gas: N_2 purge rate 60.0 ml/min), from 25 to 900 °C, at a heating rate of 10 °C/min. Three samples per species were analyzed.

Shell density measurement. Blocks of 1.0 x 3.0 cm were cut from the central portions of the right valves and weighed using Mettler Toledo XP26DR Microbalance (Mettler Toledo, LLC, Columbus, OH, USA). The volume of the samples was assessed using the liquid displacement technique in 5 ml graduated cylinders. Five samples per species were measured.

FTIR spectroscopy. Hemocytes isolated from the pooled hemolymph of 10 oysters were resuspended in 4 ml Alsever's solution and layered onto 10 ml of the 10% sucrose in Alsever's solution. Cells were purified by centrifugation for 30 min at 550×*g*, 4°C. The resulting pellet was resuspended in 1 ml of the 10% sucrose-Alsever's solution, vigorously vortexed for 20 sec, mixed with 4.0% NaOCl (1:2 v/v hemocyte suspension to NaOCl ratio), and centrifuged for 90 s at 7000×*g*. The supernatant was removed and replaced with 2.5% NaOCl. After 20 min incubation at room temperature, the samples were centrifuged for 5 min at 8000×*g* and rinsed with ultra-pure water adjusted to pH 10 with NaOH. The tubes were flash frozen in liquid nitrogen and freeze dried overnight (Labconco Freezone 4.5, Kansas City, MO, USA). Dry samples were mixed with KBr, pressed into pellets and studied using FTIR spectrometer (Broker Vertex 70, Billerica, MA, USA) in the transmission mode. For shells, material from the central portions of left valves of five oysters of each species were ground and pressed in KBr pellets. Pellets were analyzed using a FTIR spectrometer (Bruker Vertex 70, Bruker, Billerica, MA) in a transmittance mode with the resolution of 4 cm^{-1} and 128 scans per sample. Absorbance spectra were processed using Spectrum 5.1 software (Perkin Elmer, Shelton, CN). The 600-1000 cm^{-1} regions of the spectra were isolated, baseline corrected and normalized, and the positions and heights of absorption peaks of $\nu4$ and $\nu2$ vibrational bands were measured. The $\nu4/\nu2$ band intensity ratio is inversely proportional to calcite crystal and is commonly used as a proxy for the crystallinity of the mineral phase (Beniash et al., 1997; Gueta et al., 2007).

High resolution transmission electron microscopy (HR-TEM) and selected area electron diffraction (SAED). The samples were prepared in a way similar to the procedure for FTIR spectroscopy. Dry samples were resuspended in a small volume of ethanol and mounted on carbon coated Ni grids. The samples were studied using Jeol 2200 high resolution TEM, equipped with a field emission gun, in the bright field and SAED modes at the accelerating voltage of 200 KV.

Microhardness. Blocks (1 cm x 1 cm) were cut from the central portion of the right valves from five Pacific (*C. gigas*) and five eastern (*C. virginica*) oysters with the shell length of 6-8 cm. The blocks were mounted in Epofix fast curing epoxy resin (EMS, Hatfield, PA, USA) and left to polymerize for 24 h at room temperarure. The blocks were trimmed with a water-cooled slow speed saw (IsoMet, Buehler, Lake Bluff, IL, USA) and polished in the transverse plane along the long axis of the shell using Metadi diamond suspensions down to 0.25 µm (Buehler, Lake Bluff, IL, USA) in a saturated $CaCO_3$ solution. The microhardness tests were conducted using a microindenter (IndentaMet 1104, Buehler, Lake Bluff, IL, USA) at 0.245 N load and 5 sec dwelling time using Vickers indenter tip. Indentations were made in the middle of the shells' foliated layer. Five indentations were made per sample at least 100 µm away from other indents. Data from five indentantions were averaged for each shell sample to obtain a biological replicate.

Three-point bending flexural modulus and stiffness. Blocks of shell mineral (1.5 cm x 4.5 cm) were cut from the central portion of the right valves from five Pacific (*C. gigas*) and five Eastern (*C. virginica*) oysters with the total shell length of 6-8 cm. The three-point bending tests were conducted with an electronic universal mechanical testing machine (Instron 5566, Norwood, MA, USA). The applied velocity of the bending load was 1 mm min^{-1}, static load 5 kN, pre-load 0.5N and support span 22 mm. Five measurements of stiffness obtained from the same shell were averaged and used as a biological replicate.

Scanning electron microscopy (SEM). Blocks of shell (1 cm x 1 cm) were cut from the central portion of the right valves from five Pacific and five Eastern oysters, mounted in Epofix fast curing epoxy resin (EMS, Hatfield, PA, USA) and allowed to polymerize for 24 h at room temperature. The blocks were trimmed with a water cooled slow speed saw (IsoMet, Buehler, Lake Bluff, IL, USA), polished in the transverse plane along the long axis of the shell using Metadi diamond suspensions (Buehler, Lake Bluff, IL, USA) down to 0.25 µm diamond particle size in saturated $CaCO_3$ solution, and sputter coated with gold under vacuum (Anatech Hummer 10.2, Smyrna, DE, USA). The samples were examined by field-emission scanning electron microscopy (ZEISS Sigma 500 VP FE-SEM with Oxford Aztec X-EDS, Oxford, UK) at 15 kV.

Statistical analyses. One- and two-way ANOVA was used to test the effects species on the studied traits (Tables 1 and 2). For ion ratios based on the NanoSIMS analyses, cell size was included as a covariate to correct for the potential cell size and/or margin effects. The average cell size of the NanoSIMS samples was similar for the two studied species ($P>0.05$) (4.2±0.7 µm, N=19 and 4.6±0.4 µm, N=52 for *C. gigas* and *C. virginica*, respectively). Prior to analyses, data were tested for normality and homogeneity of variance by Kolmogorov-Smirnoff and Levene's tests, respectively, and normalized as needed using Box-Cox common transforming method. Fisher's Least Significant Differences (LSD) tests were used for planned post-hoc comparisons of the differences between the pairs of means of interest. Differences were considered significant if the probability of Type I error was less than 0.05. The data are presented as means ± standard error of the mean (SEM) unless indicated otherwise. Pearson correlation analysis was conducted to assess correlations between mRNA levels of target genes, tissue types and species. Principal Component Analysis (PCA) was used to reduce the dimensionality of the data set and determine the groups of molecular traits (gene transcription profiles) that distinguish the different tissue types and/or species. The correlation analysis and the PCA were conducted on raw (non-transformed) data. All statistical analyses were performed with OriginPro 2015 software package (Northhampton, MA).

RESULTS

Genes involved in ion and acid-base regulation. Tissue-specific expression of carbonic anhydrase (CA) isoforms differed between the two studied congeners (Fig. 1A-C; Table 1). CAI was expressed at relatively low levels (0.5-0.6 CAI to β-actin ratios) in all studied tissues of *C. gigas* (Fig. 1A). In *C. virginica*, CA I mRNA expression was low in hemocytes and the mantle, but considerably higher (~8.3 CAI to β-actin ratio) in the gill (Fig. 1A). When compared between the two studied species, CAI mRNA levels were considerably higher in the gills of *C. virginica* compared with those of *C. gigas* (Fig 1A). In contrast, CA XIV was highly expressed in the mantle of *C. gigas* (52-86 CAI to β-actin ratio) exceeding the respective levels in hemocytes and the gill by 40-66-fold (Fig. 1C). In *C. virginica*, CA XIV also tended to be more highly expressed in the mantle compared with other tissues (~3 CA XIV to β-actin ratio in the mantle vs. 0.5-1 in hemocytes and the gill) (Fig. 1 C). When compared among the species, CA XIV mRNA levels were significantly higher in the mantle of *C. gigas* compared with that of *C. virginica* (Fig. 1C). mRNA expression of CA II was similar in all studied tissues and between *C. gigas* and *C. virginica* (Fig. 1B).

V-type H^+ ATPase mRNA showed similar expression levels in all studied tissues of *C. gigas* (Fig. 1D). In *C. virginica*, V-type H^+ ATPase mRNA expression in hemocytes was 2-4-fold higher than in other studied tissues ($P<0.05$). The expression levels of V-type H^+ ATPase mRNA in the hemocytes and the gills were higher in *C. virginica* than in *C. gigas*. Expression of V-type H^+ ATPase was similar in the mantle of *C. gigas* and *C. virginica* (Fig. 1 D).

In *C. gigas*, mRNA levels of Ca^{2+} ATPase Type 2C were significantly elevated in the central mantle compared to other tissues, while *in C. virginica* the mRNA levels of this gene did not differ in different tissues (Fig. 1E). Expression of Ca^{2+} ATPase Type 2C mRNA was higher in the gill (but not in other tissues) of *C. virginica* than in *C. gigas* (Fig. 1E). In contrast, mRNA levels of the plasma membrane Ca^{2+} ATPase were consistently higher *C. virginica* compared with *C. gigas* in all studied tissues (Fig. 1F).

In *C. virginica*, NHX9 and NHE3 mRNA expression in the gill was higher than in other tissues of this species (albeit this trend was only significant for NHE3, $P<0.05$), whereas in *C. gigas* the mRNA levels of these two genes showed little tissue-to-tissue variation (Fig. 1G, H). NHX9 and NHE3 transporters tended to have higher expression levels in *C. virginica* tissues compared with those of *C. gigas* (Fig. 1G, H). This species-specific difference was significant in the gill, where NHE9 and NHE3 expression was ~27 and ~7 times higher in *C. virginica* than in *C. gigas*, respectively. Overall, the interspecific differences in mRNA expression of genes involved in the ion and acid-base regulation indicate higher activity of the membrane Ca^{2+} , Na^+ and H^+ transporters in *C. virginica* compared with *C. gigas*.

ECM-related genes. In *C. gigas* and *C. virginica* mRNA expression of SLP was the highest in the mantle edge (Fig. 2A). When compared between the species, mRNA levels of SLP and nacrein were notably higher in the mantle edge of *C. virginica* compared with *C. gigas*, while in hemocytes the SLP expression was slightly but significantly higher in *C. gigas* (Fig. 2A, B). Across all tissues, the expression of fibronectin Prot3L was lower in *C.gigas* than in *C. virginica,* while the expression of fibronectin Prot2L was lower in *C. virginica* (Fig. 2C,D). Fibronectin ankyrin showed higher levels of mRNA in the mantle and/or the gill compared with the HCs in both studied species of oysters. Compared between the species, fibronectin ankyrin expression was significantly higher in all tissues of *C. virginica* (except the mantle edge where this trend was not statistically significant) (Fig. 2E). Overall, mRNA levels of SLP, fibronectin Prot3L, fibronectin ankyrin and nacrein were higher in the biomineralizing tissues (the mantle and/or HCs) of *C. virginica* compared with those of C*. gigas*. In contrast, the mRNA expression of fibronectin Prot2L was higher in the mantle of *C. gigas* compared with *C. virginica* (Fig. 2, Table 1).

Biomineralization related VEGF signaling pathway. When compared among different tissues, VEGF and VEGFR mRNA levels were higher in the mantle and the gills than in HCs of *C. virginica,* a similar albeit less pronounced trend was found in *C. gigas* (Fig. 3A, B). Overall, mRNA expression of VEGF and VEGFR were higher in the mantle and the gills of *C. virginica* compared with the respective tissues of *C. gigas* (Fig. 3A, B).

Biomineralization related enzymes. Expression levels of casein kinases (CKI and CKII) involved in the ECM protein phosphorylation (Rusenko et al., 1991; Sfeir and Veis, 1996; Veis et al., 1997) was relatively uniform across different tissues within the same species (except elevated levels of CKI in the gill of *C. virginica*) and consistently higher in *C. virginica* compared with *C. gigas* (Fig. 3). In contrast, mRNA levels of chitin synthases (CS II and CS III) were higher in the biomineralizing tissues (the mantle and/or the HCs, respectively) (Fig. 3). When compared between the species, CSII mRNA levels were higher in the mantle edge of *C. gigas* compared with *C. virginica*. Expression of CSIII in the HCs was higher and in the mantle – lower in *C. gigas* than in *C. virginica* (Fig. 3).

Immune-related functions and gene expression. Hemocyte concentrations in oyster hemolymph were slightly but significantly higher in *C. gigas* (11.9$\pm$0.7 million cells per ml, N=10) compared with *C. virginica* (9.7$\pm$0.6 million cells per ml, N=10) ($P<0.05$). Phagocytic activity was similar in *C. gigas* and *C. virginica* hemocytes (980$\pm$11 vs. 820$\pm$8 Zymozan particles per 1000 cells, N=10 and 9, respectively) ($P>0.05$). Adhesion capacity of hemocytes was high in both studied species with >96% hemocytes attached after 2 h of incubation.

Of the six studied molecular pattern-recognition genes, five (TLR2, TLR3, TLR4, mannose receptor and killer cell lectin receptor) tended to be more highly expressed in *C. gigas* compared with *C. virginica* (Fig. 5; Table 2). Among those, mRNA levels of TLR3 and killer cell lectin receptor were significantly higher in hemocytes of *C. gigas* (by ~7 and ~45-fold, respectively) than in *C. virginica* ($P<0.05$) (Fig. 4B, D; Table 2). mRNA expression of TLR2, TLR4, mannose receptor 2 and SRCR did not significantly differ between hemocytes of the two studied species (Fig. 5A, C, E, F).

Expression levels of mRNA encoding big defensin, complement component 3 and TNF were ~433, ~6 and ~4 fold higher, respectively, in the hemocytes of *C. gigas* compared with *C. virginica* (Fig. 5G-I). The mRNA expression of C-lectin was similar in the hemocytes of both studied species (Fig. 5J). mRNA expression level of integrin was similar in two studied species ($p=0.07$, Table 2).

Integration of the transcriptome data using principal component and correlation analyses. Principal component analysis (PCA) of species and tissue specific variation in expression of biomineralization-related genes showed that the species had a relatively strong loading in the 1st principal component, which explains 41% of variation (Fig. 5A, Supplementary Table 2). The 2nd principal component, explaining 15% of variation, had a very strong loading associated with the tissue type. Interestingly, both mantle locations (ME and MC) clustered together, while gills clustered with hemocytes (Fig. 5A, Supplementary Table 2). Pearson correlation analysis revealed that higher gene expression levels of multiple genes were associated with *C. virginica* (Supplementary Table 3). Specifically, statistically significant positive correlations were found between expression of 10 out of 18 studied biomineralization-related genes and *C. virginica*, while higher expression of only two genes (CA14 and fibronectin Prot2L) was associated with *C. gigas*.

When only hemocytes were considered in the analysis, species showed a strong loading in the 1st principal component, which explains 44% of variation (Fig. 5B; Supplementary Table 4). PCA analysis of the expression of biomineralization-related and immune genes showed a clear separation of *C. gigas* and *C. virginica* hemocytes with higher expression of the molecular pattern recognition genes (except SRCR) as well as humoral and inflammation-related factors in hemocytes of *C. gigas* compared with *C. virginica* (Fig. 5B, Supplementary Table 3). High expression of cell-matrix interacting genes such as β-integrin and fibronectin-ankyrin was associated with *C. virginica*. Moreover, expression of casein kinases and ionoreguatory genes was positively associated with *C. virginica* (Fig. 5B). Based on the Pearson correlation analysis, expression of five genes tentatively associated with biomineralization, pH control and ion transport (CK1, VEGFR, NHX9, PM Ca ATPase, V type H^+ ATPase) was strongly and positively correlated with *C. virginica* (Supplementary Table 5). Expression of the genes potentially associated with defense (TLR3, Cq3, TNF, defensin) and cell adhesion (C-Type Lectin and fibronectin Prot 2L) positively correlated with C*. gigas* (Supplementary Table 5).

Mineral content of hemocytes.

<u>*Determination of total calcium content by ICP-MS.*</u> Calcium content was significantly lower in the total hemocyte population of *C. gigas* compared with *C. virginica* (0.41±0.028 nmole $cell^{-1}$ vs 0.72±0.09 nmole $cell^{-1}$; P=0.02) (Fig. 6A). This was also reflected in the significantly lower Ca content of individual fractions (H1-H4) of *C. gigas* hemocytes compared to those of *C. virginica*. In *C. gigas* as well as *C. virginica,* Ca content of hemocyte increase from the lightest to the heaviest hemocyte fraction, and this trend was more pronounced in *C. gigas* (Fig. 6A).

Determination of mineral phases in hemocytes by FTIR and HR-TEM. FTIR analysis revealed that the mineral phase from the hemocytes of *C. gigas* and *C. virginica* consists of calcium carbonate, predominantly calcite (Fig. 6B, C). Notably, different preparations of the mineral phase from replicate samples of hemocytes from the same species showed variations in the spectra of the mineral (Suppl. Fig. 1). Our HR TEM/SAED studies identified multiple mineral phases of $CaCO_3$ in hemocytes including amorphous calcium carbonate (ACC), calcite, dolomite and vaterite (Fig. 7). These data indicate that the calcium carbonate mineral inside oyster hemocytes is highly unstable, potentially amorphous and that it spontaneously transforms into other calcium carbonate phases (such as calcite) during the preparation procedure.

Distribution and density of Ca in hemocytes by NanoSIMS. Analysis of the NanoSIMS maps showed that the ratios of the intracellular Ca/Na and Mg/Na signals (indicative of the cellular Ca and Mg content, respectively) were ~2.7-3-fold lower in hemocytes of *C. gigas* compared to those of *C. virginica* ($P<0.001$ and $P=0.003$ for Ca/Na and Mg/Na ratios, respectively) (Fig. 8). Larger hemocytes contained relatively more Ca and Mg compared with the smaller ones as demonstrated by the significant positive effects of the cell size (used as a covariate in ANCOVA) on Ca/Na and Mg/Na ratios ($P=0.002$ and $P<0.001$, respectively). The ratio of Ca/Mg signal was higher in larger hemocytes ($P<0.001$ for the cell size used as a covariate in ANCOVA) but not significantly different between the species ($P>0.05$). NanoSIMS images of oyster hemocytes with overlapping hotspots of Ca and Mg (Fig. 8) and Ca and O (Suppl. Fig. 2) are consistent with the presence of $CaCO_3$ mineral in oyster hemocytes.

Overall, Ca content analysis revealed that hemocytes of *C. virginica* carry more calcium and that in both species the heaviest (H4) hemocyte fraction contains more Ca than others. Furthermore, the results of FTIR and diffraction analyses reveals that the mineral fraction of oyster hemocytes contains several mineral phases of $CaCO_3$.

Compositional, mineralogical and mechanical properties of the shells.

Mineralogical analysis. FTIR analysis of the oyster shells indicated that in both studied species the major mineral fraction of the shell is calcite indicated by the positions of ν_4 (712 cm^{-1}), ν_2 (878 cm^{-1}) and ν_3 (1420 cm^{-1}) absorbance bands (Andersen and Brecevic, 1991) (Fig. 9A,B). The ν_2/ν_4 peak ratio [a measure of crystallinity of calcite (Beniash et al., 1997; Gueta et al., 2007)] was significantly higher in *C. gigas* than in *C. virginica* shells (3.5±0.30 vs. 2.2±0.07; $P=0.002$) indicating that mineral in *C. gigas* shells is less crystalline than in those of *C. virginica*.

Ultrastructural and mechanical analysis. SEM analysis of the foliated layer revealed similarity of the overall ultrastructure of the shells of *C. gigas* and *C. virginica* (Suppl. Fig 3). However, the thickness of the laths in the shells of *C. gigas* was significantly lower than in *C. virginica* (187 ± 22 nm vs. 251 ± 24 nm; P=0.03) (Fig. 9C). Similarly, the microhardness of the foliated layers of the shells was significantly lower in *C. gigas* than in *C. virginica* (152 ± 9 VH vs. 206 ± 1.3 VH; P<0.005). The three-point bending test of revealed that the shells of *C. virginica* were significantly stiffer than shells of *C. gigas* (2.4±0.41 $x10^6$ vs N m^{-1} 0.42 ± 0.22 $x10^6$ N m^{-1}; P<0.0001) (Fig. 9). Similarly, the maximum compressive load was lower in *C. gigas* shells compared to those of *C. virginica* (2.5 ± 0.56 $x10^5$ N m^{-1} vs. 9.35 ± 5.5 $x10^5$ N m^{-1}; P=0.05) (Fig. 9). Taken together these data reveal differences in shell mineralogy and ultrastructure between two species studied and show that the shells of *C. gigas* are mechanically inferior to those of *C. virginica*.

Compositional analysis. TGA analysis did not show any significant differences in the organic content of the shells between *C. gigas* and *C. virginica* (1.95 ± 0.08% vs. 3.12 ± 1.01%; p=0.18) (Fig. 9). Notably, the density of the *C. gigas* shells was significantly lower than that of *C. virginica* (2.0 ± 0.59 g ml^{-1} vs. 3.2 ± 0.37 g ml^{-1}, P=0.005) (Fig. 9). Taken together, the results of TGA and density analyses suggest that the shells of *C. gigas* are more porous than those of *C. virginica*.

DISCUSSION

Shell mineralogy, structural and mechanical properties in two oyster congeners differ

Despite similar shell morphology, the mineralogical, compositional and mechanical properties of the shells dramatically differ between the two closely related species of oysters, *C. virginica* and *C. gigas*. FTIR analysis revealed that calcite in the shells of *C. gigas* is less crystalline than in *C. virginica* suggesting that the kinetics of crystal maturation process in these shells is slower, or that they contain more ACC (Beniash et al., 1997; Gueta et al., 2007). These differences in mineral crystallinity can affect the mechanical properties of the crystals and influence shell hardness. This suggestion is borne out by the results of the mechanical analyses showing considerably lower shell microhardness in *C. gigas* compared with *C. virginica*. It is worth noting that the shell microhardness in oysters is a plastic trait and can change depending on the growing conditions. Our earlier studies (Beniash et al., 2010) showed that the shell microhardness of *C. virginica* juveniles grown under the the reduced pH (elevated CO_2) was significantly lower than the shell microhardness of the juveniles grown under the normal conditions. Based on the shell microstructural analysis, we hypothesized that the differences in the microhardness of the shells grown at the normal and elevated CO_2 levels are associated with the differences in the lath thickness

(Beniash et al., 2010). In this earlier study, the shells with higher microhardness were made of thinner laths (Beniash et al., 2010). In contrast, in the present study the shells with thicker laths were harder. These results suggest that it is not the lath thickness (as we speculated earlier) but other factors that affect the microhardess of the lath layers. These differences can be due to the interfacial properties of the laths or the adhesive properties of the organic matrix. It is also possible that the higher hardness of *C. virginica* shells is associated with the higher mineral crystallinity as assessed by FTIR. Bulk mechanical properties of the shells such as stiffness and maximum load were also significantly higher in *C. virginica* compared with *C. gigas*. We attribute these differences to the higher porosity of *C. gigas* shells. Taken together, these data demonstrate that the shells of *C. virginica* are mechanically superior to those of *C. gigas* on both micro- and macroscale.

Expression of biomineralization-related genes in the mantle and the gills is higher in C. virginica than C. gigas

Biomineralization of oyster shells is a complex process involving coordinated action of multiple organs (Gardner et al., 2011; Ivanina et al., 2017; Johnstone et al., 2015; Li et al., 2016). Our data indicate stronger expression of acid-base and ionoregulatory genes in different tissues (including mantle, gills and hemocytes) of *C. virginica* compared with *C. gigas*. This includes several isoforms of carbonic anhydrases (except CA XIV that is more highly expressed in the mantle of *C. gigas*), an ATP-dependent proton pump (V Type H^+ ATPase) and sodium-proton exchangers that that play a crucial role in acid-base homeostasis by regulating intra- and extracellular pH and bicarbonate concentrations (Larsen et al., 2014). Notably, the transcripts of many acid-base and ion regulation related genes were as (or more) highly expressed in the gill as in the biomineralization-specialized tissues such as the mantle or hemocytes. This is consistent with the important role of the gill in the systemic acid-base and ion homeostasis (Larsen et al., 2014). Furthermore, the plasma membrane Ca^{2+} ATPase involved in intracellular Ca^{2+} homeostasis is also more highly expressed in the different tissues of *C. virginica* compared with *C. gigas*. Higher expression of the genes involved in acid-base regulation and Ca^{2+} transport may help create a favorable milieu for biomineralization due to a better regulation of pH and $CaCO_3$ saturation levels in the extrapallial cavity and at tissue-shell interface of *C. virginica* compared with *C. gigas* (Holcomb et al., 2014; Ramesh et al., 2017; Venn et al., 2013).

Expression of the ECM-related genes shows complex profiles among different tissues in the two studied species. Generally, *C. virginica* expresses higher mRNA levels of fibronectins (fibronectin ankyrin and fibronectin Prot3L but not Prot 2L) as well as the genes associated with ECM maturation (casein kinases) and SLP in the mantle and/or the gill tissues. The tissue-specific patterns of expression of chitin synthases and nacrein are more variable between the two studied tissues. Interestingly, transcripts of some ECM-related proteins (including fibronectins and casein kinases) are highly abundant in the gills of oysters, an organ not traditionally associated with biomineralization. This finding is consistent with

earlier reports of de-localized synthesis of ECM proteins in oysters and their subsequent transport in the blood to the biomineralization sites (Wang et al., 2013). This might indicate that the biomineralization in mollusks has a greater contribution from the organ systems other than mantle thus challenging the classical biomineralization model.

Notably, the genes involved in cell-cell signaling (VEGF and VEGFR) showed higher transcript levels in mantle and gill tissues of *C. virginica* compared with *C. gigas*. VEGF and its receptor have been implicated in biomineralization of invertebrates such as sea urchins, where VEGF regulates migration of the skeletogenic primary mesenchymal cells (Adomako-Ankomah and Ettensohn, 2014; Duloquin et al., 2007) and growth of the calcitic spicules (Knapp et al., 2012). In *C. gigas*, subpopulations of hemocytes specialized on biomineralization also expressed higher VEGF and VEGFR mRNA levels compared to the immune-specialized hemocytes thus underscoring the potential role of VEGF in biomineralization (Ivanina et al., 2017). However, our recent study in *C. gigas* juveniles showed that while chemical interference with the VEGF signaling modulates biomineralization, VEGF inhibition does not result in disrupted skeletogenesis (Ivanina et al., in review). While higher expression of VEGF and VEGFR in *C. virginica* compared with *C. gigas* is consistent with the pattern found for most studied biomineralization-related genes, the functional implications of VEGF for oyster biomineralizaton remain speculative due to the poorly defined role of this signaling pathway in the mollusks.

Hemocytes of C. virginica contain higher amounts of Ca than those of C. gigas

Our ICP-MS and NanoSIMS studies revealed large differences in the Ca content of the different fractions of hemocytes in both species, with the largest and heaviest hemocytes containing the highest Ca amount. Notably, in our earlier study we found that the free Ca^{2+} concentration in the heaviest hemocyte fraction is the lowest (Ivanina et al., 2017). These results suggest that this hemocyte fraction contains bound Ca potentially in a form of $CaCO_3$ mineral. Importantly, Ca content was significantly higher in the total hemocyte populations, as well as across different hemocyte size fractions, in *C. virginica* than in *C. gigas*. These results are in a good agreement with the results of our transcriptome analysis, showing that the expression of the biomineralization-related genes (especially those involved in the ion egulation and Ca transport) is higher in hemocytes of *C. virginica*. This might imply that biomineralization processes in *C. virginica* are more active than in *C. gigas* thereby contributing to the superior shell quality of *C. virginica* compared with *C. gigas*.

Mineral sequestration and cellular transport involve metastable calcium carbonate mineral phases

The ability of oyster hemocytes (especially those of *C. virginica*) to accumulate significant amounts of Ca without the associated Ca^{2+} toxicity may be achieved by storing intracellular Ca^{2+} in $CaCO_3$ mineral particles. Our FTIR spectroscopy and HR-TEM analyses confirmed the presence of calcium carbonate mineral particles in hemocytes. Importantly, several $CaCO_3$ mineral phases were identified in hemocytes, including the least thermodynamically stable ACC, suggesting that intracellular $CaCO_3$ is stored as a highly unstable ACC, which is transformed into other phases during the experimental preparation and/or deposition on the growing shell. The presence of $CaCO_3$ in oyster hemocytes demonstrated in our present study is consistent with the earlier reports of $CaCO_3$ in bivalve hemocytes assessed by microscopy (Li et al., 2016; Mount et al., 2004). The biomineralization strategy involving mineral ion sequestration by cells away from the mineralization site coupled with the transport of these ions in a form of a metastable mineral phase were identified in vertebrates (Akiva et al., 2015; Kerschnitzki et al., 2016) and echinoderms (Vidavsky et al., 2014; Vidavsky et al., 2015). Our results suggest that this strategy might be more widespread than was previously thought.

Immune-and biomineralization-related traits of hemocytes: Evidence of trade-off?

Our study showed considerable differences in the gene expression patterns and functional characteristics of hemocytes of the two closely related species of oysters indicating that the hemocytes of *C. gigas* are more strongly specialized on the immune defense, while *C. virginica* hemocytes possess more active ionoregulatory and Ca transport mechanisms.

The pathogen recognition system of *C. gigas* hemocytes is more highly expressed than in *C. virginica*. Immune surveillance in oysters, like in other organisms lacking adaptive immunity, entirely depends on the germ-line encoded pattern recognition receptors (PRRs) that recognize pathogen-associated molecular patterns (PAMPs) from various microbes (Ward and Rosenthal, 2014). *C. gigas*, the only Ostreidae species for which the full genome data are available, shows massive expansion and diversification of the PRRs genes compared with vertebrates, insects or cnidarians, likely reflecting adaptation to the abundant and diverse microbial challenges in estuarine and coastal habitats (Zhang et al., 2015). Our present study shows that circulating hemocytes of *C. gigas* express higher levels of several key PRR-encoding genes compared with a closely related but less disease resistant *C. virginica* (Barbosa Solomieu et al., 2015; Elston, 1993; Ford, 1996). This includes three isoforms of TLR receptors (TLR2, TLR3 and TLR3) belonging to a family of transmembrane receptors specialized on the recognition the viral and bacterial PAMPs (Ward and Rosenthal, 2014; Zhang et al., 2015). Functional studies showed that oyster

TLRs (including TLR2, 3, and 4) are strongly activated by bacterial PAMPs such as the heat-killed *Vibrios,* bacterial lipopolysaccharide and lipoproteins (Zhang et al., 2013). The oyster TLR3 also responds to dsRNA (albeit more weakly than to bacterial PAMPs) and thus may also be involved in virus recognition (Zhang et al., 2013). Interestingly, elevated expression of TLRs in *C. gigas* hemocytes goes hand-in-hand with high expression of the tumor necrosis factor (TNFα), a major TLR-dependent regulator of inflammation (Parameswaran and Patial, 2010). Elevated expression of TLRs and TNFα in *C. gigas* may thus indicate higher activity of the pathogen-induced inflammatory pathways in this species compared with *C. virginica* and may contribute to higher resistance to bacterial pathogens in *C. gigas*.

Hemocytes of *C. gigas* are better equipped to fight eukaryotic pathogens than hemocytes of *C. virginica*. *C. gigas* hemocytes present considerably higher mRNA expression of PRRs involved in the recognition of eukaryotic pathogens including mannose receptor 2 (~1.5-fold higher than in *C. virginica*) and killer cell lectin-like receptor (~45-fold higher than in *C. virginica*). Mannose receptor and the killer cell lectin-like receptor belong to the family of C-type lectins with broad glycan specificity recognizing fungal PAMPs as well as other eukaryotic pathogens including protists and parasitic helminths (Llibre et al., 2016; van Die and Cummings, 2017; Vautier et al., 2012). Taken together, the species-specific transcription patterns of immune-related genes suggest that *C. gigas* hemocytes are better equipped to recognize a broad repertoire of bacterial, viral and eukaryotic pathogens compared with *C. virginica*.

The antibacterial humoral defense of hemocytes also appears to be more active in *C. gigas* than in *C. virginica*. Remarkably, the basal mRNA expression levels of a major humoral component of the immune system, the big defensin, was ~432-fold higher in *C. gigas* hemocytes compared with *C. virginica*. Big defensin is an important antimicrobial peptide (AMP) with a broad pathogen specificity and microbicidal activity against Gram-positive, Gram-negative bacteria and eukaryotic microbes (Rosa et al., 2011; Schmitt et al., 2012). In *C. gigas*, big defensins are highly inducible by exposure to bacterial infections and/or to PAMPs (Rosa et al., 2011; Schmitt et al., 2012). This inducibility, combined with the high baseline levels of big defensin, may aid *C. gigas* hemocytes in effective elimination of bacterial and protozoan pathogens. Furthermore, *C. gigas* hemocytes express considerably (~6-fold) higher mRNA levels of the complement component 3 (C3) compared with *C. virginica* hemocytes. The complement component 3 acts as a central innate immunity hub mediating opsonization and production of AMPs to eliminate the pathogens and activating the complement cascade as the first line of immune defense (Ricklin et al., 2016; Volanakis, 1990). In marine bivalves such as the mussel *Mytilus corruscus,* the razor clam *Sinonovacula constricta* and oysters *C. gigas*, C3 is stimulated by bacterial infection (*Vibrio* and *Micrococcus* species), exposure to bacterial PAMPs or toxic insults (such as dissolved copper) (Chen et al., 2018; Dong et al., 2017; Peng et al., 2017; Peng et al., 2016; Wang et al., 2017a). Highly expressed C3 system combined with the elevated expression of AMPs such

as big defensin might contribute to a more rapid activation of the humoral immune defense and more effective pathogen killing in *C. gigas* compared with *C. virginica*.

Transcriptome analysis also sheds light on the mineral sequestration and transport mechanisms by hemocytes showing strong species-specific differences in the expression of the genes involved in ion regulation and deposition of the ECM proteins. Thus, the transcripts of the genes involved in Ca^{2+}, Na^{+} and H^{+} transport (V-type H^{+} ATPase, Ca^{2+} ATPase, the plasma membrane Ca^{2+} ATPase and NHE9 sodium-proton exchanger) were consistently more highly expressed (by ~2-5 fold) in the hemocytes of *C. virginica* compared to *C. gigas*. Active ionoregulation is crucially important for bivalve hemocytes as they sequester and transport Ca^{2+} to the sites of biomineralization (Ivanina et al., 2017; Mount et al., 2004; Wang et al., 2017c). This poses major physiological challenges to hemocytes as they need to carry large quantities of Ca^{2+} to the sites of shell biomineralization, while at the same time avoiding cytotoxicity. This might explain higher expression of the genes involved in the maintenance of intracellular Ca^{2+} levels (notably, PM Ca^{2+} ATPase) (Brini and Carafoli, 2011). In vertebrates and *Drosophila* PM Ca^{2+} ATPase is mostly responsible for the efflux of Ca^{2+} from the cells to regulate the household Ca^{2+} homeostasis (Brini and Carafoli, 2011). If similar mechanisms exist in oysters, high expression of PM Ca^{2+} ATPase in *C. virginica* hemocytes may aid in regulation of the intracellular free Ca^{2+} levels of the cells that accumulate and transport Ca to the biomineralization sites. Transcripts of the genes encoding casein kinases involved in phosphorylation of ECM proteins were ~7-10 times more abundant in *C. virginica* hemocytes. In contrast, genes encoding ECM proteins (including SLP, nacrein and fibronectins) were similarly expressed in the hemocytes of the two studied species of oysters.

Conclusions and perspectives

Our study demonstrates the molecular and cellular basis of the species-specific differences in important fitness-related phenotypes (disease resistance and exoskeleton properties) between two closely related and ecologically similar species of oysters. The hemocytes of the two studied species are multifunctional cells, yet transcriptomic and mineralogical profiles of the hemocytes show predominant specialization on immune defense (*C. gigas*) or ion regulation and Ca transport (*C. virginica*). To the best of our knowledge, our data provide the first demonstration that hemocytes contain metastable calcium carbonate mineral phases, which is potentially transported to the sites of mineralization, as well as further evidence that only certain fractions of hemocytes are responsible for mineral sequestration and transport. Higher investment in biomineralization function is also apparent from the elevated expression of biomineralization-related genes in other organs (the mantle and the gills) of *C. virginica* compared to *C. gigas*. These species-specific transcriptomic differences in biomineralizing (the mantle and the hemocytes) and ionoregulatory (the gills) organs are manifested in oysters' phenotype as superior

protective properties of the exoskeleton in *C. virginica* (shown in this study) or more effective immune defense in *C. gigas* (Barbosa Solomieu et al., 2015; Elston, 1993; Goedken et al., 2005; Salvi et al., 2014). Further studies are needed to gain insights into the evolutionary pathways and selective pressures that resulted in the species-specific phenotypic specialization on internal (immunity) or external (exoskeleton) protection and assess whether it is based on true energetic or resource trade-off.

ACKNOWLEDGEMENTS

The work was supported by the U.S. National Science Foundation awards IOS-1557870 and IOS-1557551 to IMS, AVI and EB. Ifra Malik's research experience was supported by REU supplement for the grant IOS-1557551. The NanoSIMS instrument was funded by the German Federal Ministry of Education and Research (BMBF), grant identifier 03F0626A. We thank Annett Grüttmüller for performing the routine NanoSIMS operations. The high-resolution TEM studies were carried out at the Nanofabrication and Nanocharacterization Facility, Peterson Institute for Nanoscience and Engineering.

References

Adomako-Ankomah, A. and Ettensohn, C. A. (2014). Growth factors and early mesoderm morphogenesis: Insights from the sea urchin embryo. *genesis* **52**, 158-172.

Akiva, A., Malkinson, G., Masic, A., Kerschnitzki, M., Bennet, M., Fratzl, P., Addadi, L., Weiner, S. and Yaniv, K. (2015). On the pathway of mineral deposition in larval zebrafish caudal fin bone. *Bone* **75**, 192-200.

Allam, B. and Pales Espinosa, E. (2016). Bivalve immunity and response to infections: Are we looking at the right place? *Fish & Shellfish Immunology* **53**, 4-12.

Andersen, F. A. and Brecevic, L. (1991). Infrared spectra of amorphous and crystalline calcium carbonate. *Acta Chem. Scand* **45**, 1018-1024.

Arumugan, M., Romestand, B., Torreilles, J. and Roch, P. (2000). In vitro production of superoxide and nitric oxide (as nitrite and nitrate) by *Mytilus galloprovincialis* haemocytes upon incubation with PMA or laminarin or during yeast phagocytosis. *Eur J Cell Biol* **79**, 513-519.

Barbosa Solomieu, V., Renault, T. and Travers, M.-A. (2015). Mass mortality in bivalves and the intricate case of the Pacific oyster, Crassostrea gigas. *Journal of Invertebrate Pathology* **131**, 2-10.

Beck, M. W., Brumbaugh, R. D., Airoldi, L., Carranza, A., Coen, L. D., Crawford, C., Defeo, O., Edgar, G. J., Hancock, B., Kay, M. C. et al. (2011). Oyster reefs at risk and recommendations for conservation, restoration, and management. *Bioscience* **61**, 107-116.

Ben-Horin, T., Bidegain, G., Huey, L., Narvaez, D. A. and Bushek, D. (2015). Parasite transmission through suspension feeding. *Journal of Invertebrate Pathology* **131**, 155-176.

Beniash, E., Aizenberg, J., Addadi, L. and Weiner, S. (1997). Amorphous calcium carbonate transforms into calcite during sea urchin larval spicule growth. *Proceedings of the Royal Society of London Series B* **264**, 461-465.

Beniash, E., Ivanina, A., Lieb, N. S., Kurochkin, I. and Sokolova, I. M. (2010). Elevated levels of carbon dioxide affect metabolism and shell formation in oysters *Crassostrea virginica*. *Marine Ecology Progress Series* **419**, 95-108.

Brini, M. and Carafoli, E. (2011). The Plasma Membrane Ca(2+) ATPase and the Plasma Membrane Sodium Calcium Exchanger Cooperate in the Regulation of Cell Calcium. *Cold Spring Harbor Perspectives in Biology* **3**, a004168.

Chen, Y., Xu, K., Li, J., Wang, X., Ye, Y. and Qi, P. (2018). Molecular characterization of complement component 3 (C3) in Mytilus coruscus improves our understanding of bivalve complement system. *Fish Shellfish Immunol* **76**, 41-47.

Chu, F.-L. E., Volety, A. K. and Constantin, G. (1996). A comparison of Crassostrea gigas and C. virginica: effects of temperature and salinity on susceptibility to the protozoan parasite, Perkinsus marinus. *Journal of Shellfish Research* **15**, 375-380.

Defer, D., Desriac, F., Henry, J., Bourgougnon, N., Baudy-Floc'h, M., Brillet, B., Le Chevalier, P. and Fleury, Y. (2013). Antimicrobial peptides in oyster hemolymph: The bacterial connection. *Fish & Shellfish Immunology* **34**, 1439-1447.

Dong, W., Chen, Y., Lu, W., Wu, B. and Qi, P. (2017). Transcriptome analysis of Mytilus coruscus hemocytes in response to Vibrio alginnolyficus infection. *Fish Shellfish Immunol* **70**, 560-567.

Duloquin, L., Lhomond, G. and Gache, C. (2007). Localized VEGF signaling from ectoderm to mesenchyme cells controls morphogenesis of the sea urchin embryo skeleton. *Development* **134**, 2293-2302.

Elston, R. A. (1993). Infectious diseases of the Pacific oyster, Crassostrea gigas. *Annual Review of Fish Diseases* **3**, 259-276.

Ford, S. and Smolowitz, R. (2007). Infection dynamics of an oyster parasite in its newly expanded range. *Marine Biology* **151**, 119-133.

Ford, S. E. (1996). Range extension by the oyster parasite Perkinsus marinus into the northeastern United States: Response to climate change? *Journal of Shellfish Research* **15**, 45-56.

Foster, B., Grewal, S., Graves, O., Hughes Jr, F. M. and Sokolova, I. M. (2011). Copper exposure affects hemocyte apoptosis and *Perkinsus marinus* infection in eastern oysters *Crassostrea virginica* (Gmelin). *Fish & Shellfish Immunology* **31**, 341-349.

Gardner, L., Mills, D., Wiegand, A., Leavesley, D. and Elizur, A. (2011). Spatial analysis of biomineralization associated gene expression from the mantle organ of the pearl oyster Pinctada maxima. *BMC Genomics* **12**, 455.

Goedken, M., Morsey, B., Sunila, I. and De Guise, S. (2005). Immunomodulation of *Crassostrea gigas* and *Crassostrea virginica* cellular defense mechanisms by *Perkinsus marinus*. *Journal of Shellfish Reasearch* **24**, 487-496.

Gourdon, I., Guerin, M. C., Torreilles, J. and Roch, P. (2001). Nitric Oxide Generation by Hemocytes of the

Mussel Mytilus galloprovincialis. *Nitric Oxide-Biology and Chemistry* **5**, 1-6.

Gueta, R., Natan, A., Addadi, L., Weiner, S., Refson, K. and Kronik, L. (2007). Local atomic order and infrared spectra of biogenic calcite. *Angewandte Chemie, International Edition* **46**, 291-294.

Guo, X., He, Y., Zhang, L., Lelong, C. and Jouaux, A. (2015). Immune and stress responses in oysters with insights on adaptation. *Fish & Shellfish Immunology* **46**, 107-119.

Hellio, C., Bado-Nilles, A., Gagnaire, B., Renault, T. and Thomas-Guyon, H. (2007). Demonstration of a true phenoloxidase activity and activation of a ProPO cascade in Pacific oyster, *Crassostrea gigas* (Thunberg) in vitro. *Fish & Shellfish Immunology* **22**, 433-440.

Holcomb, M., Venn, A. A., Tambutté, E., Tambutté, S., Allemand, D., Trotter, J. and McCulloch, M. (2014). Coral calcifying fluid pH dictates response to ocean acidification. *Scientific Reports* **4**, 5207.

Hughes, F. M., Foster, B., Grewal, S. and Sokolova, I. M. (2010). Apoptosis as a host defense mechanism in Crassostrea virginica and its modulation by Perkinsus marinus. *Fish & Shellfish Immunology* **29**, 247-257.

Ivanina, A. V., Falfushynska, H. I., Beniash, E., Piontkivska, H. and Sokolova, I. M. (2017). Biomineralization-related specialization of hemocytes and mantle tissues of the Pacific oyster Crassostrea gigas. *Journal of Experimental Biology* **220**, 3209-3221.

Ivanina, A. V., Hawkins, C. and Sokolova, I. M. (2014). Immunomodulation by the interactive effects of cadmium and hypercapnia in marine bivalves Crassostrea virginica and Mercenaria mercenaria. *Fish & Shellfish Immunology* **37**, 299-312.

Johnstone, M. B., Gohad, N. V., Falwell, E. P., Hansen, D. C., Hansen, K. M. and Mount, A. S. (2015). Cellular orchestrated biomineralization of crystalline composites on implant surfaces by the eastern oyster, *Crassostrea virginica* (Gmelin, 1791). *Journal of Experimental Marine Biology and Ecology* **463**, 8-16.

Kerschnitzki, M., Akiva, A., Ben Shoham, A., Koifman, N., Shimoni, E., Rechav, K., Arraf, A. A., Schultheiss, T. M., Talmon, Y., Zelzer, E. et al. (2016). Transport of membrane-bound mineral particles in blood vessels during chicken embryonic bone development. *Bone* **83**, 65-72.

Knapp, R. T., Wu, C. H., Mobilia, K. C. and Joester, D. (2012). Recombinant Sea Urchin Vascular Endothelial Growth Factor Directs Single-Crystal Growth and Branching in Vitro. *Journal of the American Chemical Society* **134**, 17908-17911.

Kocot, K. M., Aguilera, F., McDougall, C., Jackson, D. J. and Degnan, B. M. (2016). Sea shell diversity and rapidly evolving secretomes: insights into the evolution of biomineralization. *Frontiers in Zoology* **13**, 23.

Larsen, E. H., Deaton, L. E., Onken, H., O'Donnell, M., Grosell, M., Dantzler, W. H. and Weihrauch, D. (2014). Osmoregulation and Excretion. In *Comprehensive Physiology*, vol. 4, pp. 405-573: John Wiley & Sons, Inc.

Li, S., Liu, Y., Liu, C., Huang, J., Zheng, G., Xie, L. and Zhang, R. (2016). Hemocytes participate in calcium carbonate crystal formation, transportation and shell regeneration in the pearl oyster Pinctada fucata. *Fish & Shellfish Immunology* **51**, 263-270.

Llibre, A., Klenerman, P. and Willberg, C. B. (2016). Multi-functional lectin-like transcript-1: A new player in human immune regulation. *Immunology Letters* **177**, 62-69.

MacIntyre, E. A., Earnhart, C. G. and Kaattari, S. L. (2003). Host oyster tissue extracts modulate in vitro protease expression and cellular differentiation in the protozoan parasite, *Perkinsus marinus*. *Parasitology* **126**, 293–302.

Mount, A. S., Wheeler, A. P., Paradkar, R. P. and Snider, D. (2004). Hemocyte-mediated shell mineralization in the eastern oyster. *Science* **304**, 297-300.

Parameswaran, N. and Patial, S. (2010). Tumor Necrosis Factor-α Signaling in Macrophages. *Critical reviews in eukaryotic gene expression* **20**, 87-103.

Peng, M., Niu, D., Chen, Z., Lan, T., Dong, Z., Tran, T. N. and Li, J. (2017). Expression of a novel complement C3 gene in the razor clam Sinonovacula constricta and its role in innate immune response and hemolysis. *Dev Comp Immunol* **73**, 184-192.

Peng, M., Niu, D., Wang, F., Chen, Z. and Li, J. (2016). Complement C3 gene: Expression characterization and innate immune response in razor clam Sinonovacula constricta. *Fish Shellfish Immunol* **55**, 223-32.

Perez, D. G. and Fontanetti, C. S. (2010). Hemocitical responses to environmental stress in invertebrates: a review. *Environmental Monitoring and Assessment* **177**, 437-447.

Pfaffl, M. W. (2001). A new mathematical model for relative quantification in real-time RT–PCR. *Nucleic Acids Research* **29**, e45-e45.

Ramesh, K., Hu, M. Y., Thomsen, J., Bleich, M. and Melzner, F. (2017). Mussel larvae modify calcifying fluid carbonate chemistry to promote calcification. *Nature Communications* **8**, 1709.

Rebelo, M. d. F., Figueiredo, E. d. S., Mariante, R. M., Nóbrega, A., de Barros, C. M. and Allodi, S. (2013). New insights from the oyster *Crassostrea rhizophorae* on bivalve circulating hemocytes. *PLoS ONE* **8**, e57384.

Ricklin, D., Reis, E. S., Mastellos, D. C., Gros, P. and Lambris, J. D. (2016). Complement component C3 - The "Swiss Army Knife" of innate immunity and host defense. *Immunological Reviews* **274**, 33-58.

Romestand, B., Corbier, F. and Roch, P. (2002). Protease inhibitors and haemagglutinins associated with resistance to the protozoan parasite, Perkinsus marinus, in the Pacific pyster, Crassostrea gigas. *Parasitology* **125**, 323-329.

Rosa, R. D., Santini, A., Fievet, J., Bulet, P., Destoumieux-Garzon, D. and Bachere, E. (2011). Big defensins, a diverse family of antimicrobial peptides tha follows different patterns of expression in hemocytes of the oyster *Crassostrea gigas*. *PLoS ONE* **6**, 1-11.

Rusenko, K. W., Donachy, J. E. and Wheeler, A. P. (1991). Purification and characterization of a shell matrix phosphoprotein from the american oyster. *ACS Symposium Series* **444**, 107-124.

Salvi, D., Macali, A. and Mariottini, P. (2014). Molecular Phylogenetics and Systematics of the Bivalve Family Ostreidae Based on rRNA Sequence-Structure Models and Multilocus Species Tree. *PLoS ONE* **9**, e108696.

Sanni, B., Williams, K., Sokolov, E. P. and Sokolova, I. M. (2008). Effects of acclimation temperature and cadmium exposure on mitochondrial aconitase and LON protease from a model marine ectotherm, *Crassostrea virginica*. *Comparative Biochemistry and Physiology, Part C* **147**, 101-112.

Schmitt, P., Rosa, R. D., Duperthuy, M., de Lorgeril, J., Bachère, E. and Destoumieux-Garzón, D. (2012). The Antimicrobial Defense of the Pacific Oyster, Crassostrea gigas. How Diversity may

Compensate for Scarcity in the Regulation of Resident/Pathogenic Microflora. *Frontiers in Microbiology* **3**, 160.

Sfeir, C. and Veis, A. (1996). The Membrane Associated Kinases which Phosphorylate Bone and Dentin Extracellular Matrix Phosphoproteins are Isoforms of Cytosolic CKII. *Connective Tissue Research* **35**, 215-222.

Sokolova, I. M., Sukhotin, A. A. and Lannig, G. (2011). Stress effects on metabolism and energy budgets in mollusks In *Oxidative Stress in Aquatic Ecosystems*, (ed. J. P. V.-M. Doris Abele, Tania Zenteno-Savín), pp. 263-280: John Wiley & Sons, Ltd.

Sunila, I. and LaBanca, J. (2003). Apoptosis in the pathogenesis of infectious diseases of the eastern oyster Crassostrea virginica. *Disease of Aquatic organisms* **56**, 163-170.

van Die, I. and Cummings, R. D. (2017). The Mannose Receptor in Regulation of Helminth-Mediated Host Immunity. *Front Immunol* **8**, 1677.

Vautier, S., MacCallum, D. M. and Brown, G. D. (2012). C-type lectin receptors and cytokines in fungal immunity. *Cytokine* **58**, 89-99.

Veis, A., Sfeir, C. and Chou Bing, W. (1997). Phosphorylation of the Proteins of the Extracellular Matrix of Mineralized Tissues By Casein Kinase-Like Activity. *Critical Reviews in Oral Biology & Medicine* **8**, 360-379.

Venn, A. A., Tambutté, E., Holcomb, M., Laurent, J., Allemand, D. and Tambutté, S. (2013). Impact of seawater acidification on pH at the tissue–skeleton interface and calcification in reef corals. *Proceedings of the National Academy of Sciences* **110**, 1634-1639.

Vidavsky, N., Addadi, S., Mahamid, J., Shimoni, E., Ben-Ezra, D., Shpigel, M., Weiner, S. and Addadi, L. (2014). Initial stages of calcium uptake and mineral deposition in sea urchin embryos. *Proceedings of the National Academy of Sciences of the United States of America* **111**, 39-44.

Vidavsky, N., Masic, A., Schertel, A., Weiner, S. and Addadi, L. (2015). Mineral-bearing vesicle transport in sea urchin embryos. *Journal of Structural Biology* **192**, 358-365.

Volanakis, J. E. (1990). Participation of C3 and its ligands in complement activation. *Curr Top Microbiol Immunol* **153**, 1-21.

Wang, L., Song, X. and Song, L. (2018). The oyster immunity. *Developmental & Comparative Immunology* **80**, 99-118.

Wang, L., Zhang, H., Wang, L., Zhang, D., Lv, Z., Liu, Z., Wang, W., Zhou, Z., Qiu, L., Wang, H. et al. (2017a). The RNA-seq analysis suggests a potential multi-component complement system in oyster Crassostrea gigas. *Dev Comp Immunol* **76**, 209-219.

Wang, W., Li, M., Wang, L., Chen, H., Liu, Z., Jia, Z., Qiu, L. and Song, L. (2017b). The granulocytes are the main immunocompetent hemocytes in Crassostrea gigas. *Developmental & Comparative Immunology* **67**, 221-228.

Wang, X., Li, L., Zhu, Y., Du, Y., Song, X., Chen, Y., Huang, R., Que, H., Fang, X. and Zhang, G. (2013). Oyster shell proteins originate from multiple organs and their probable transport pathway to the shell formation front. *PLoS ONE* **8**, e66522.

Wang, X., Wang, M., Jia, Z., Song, X., Wang, L. and Song, L. (2017c). A shell-formation related carbonic anhydrase in Crassostrea gigas modulates intracellular calcium against CO2 exposure: Implication for impacts of ocean acidification on mollusk calcification. *Aquatic Toxicology* **189**, 216-228.

Ward, A. E. and Rosenthal, B. M. (2014). Evolutionary responses of innate immunity to adaptive immunity. *Infect Genet Evol* **21**, 492-6.

Zhang, L., Li, L., Guo, X., Litman, G. W., Dishaw, L. J. and Zhang, G. (2015). Massive expansion and functional divergence of innate immune genes in a protostome. *Scientific Reports* **5**, 8693.

Zhang, Y., He, X., Yu, F., Xiang, Z., Li, J., Thorpe, K. L. and Yu, Z. (2013). Characteristic and Functional Analysis of Toll-like Receptors (TLRs) in the lophotrocozoan, Crassostrea gigas, Reveals Ancient Origin of TLR-Mediated Innate Immunity. *PLoS ONE* **8**, e76464.

Figures

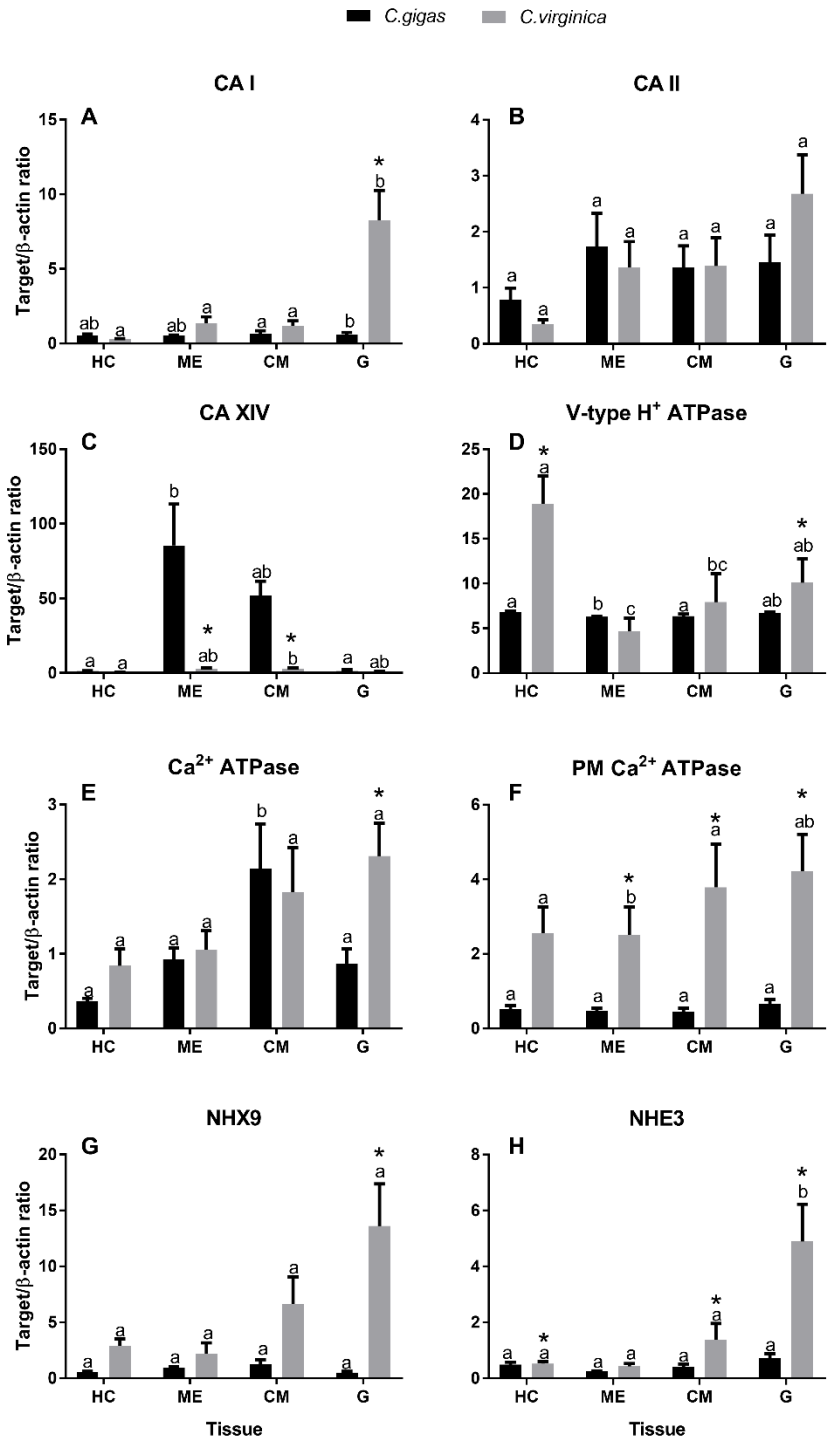

Figure 1. Expression levels of mRNA of genes involved in ion and acid-base regulation in tissues of *C. gigas* and *C. virginica*.

Gene names are shown on the figure panes. Dark bars – *C. gigas*, grey bars – *C. virginica*. Different letters indicate the values that are significantly different between different tissues within the same species ($P<0.05$). Asterisks indicate the values that are significantly different between *C. gigas* and *C. virginica* in the same tissue ($P<0.05$).

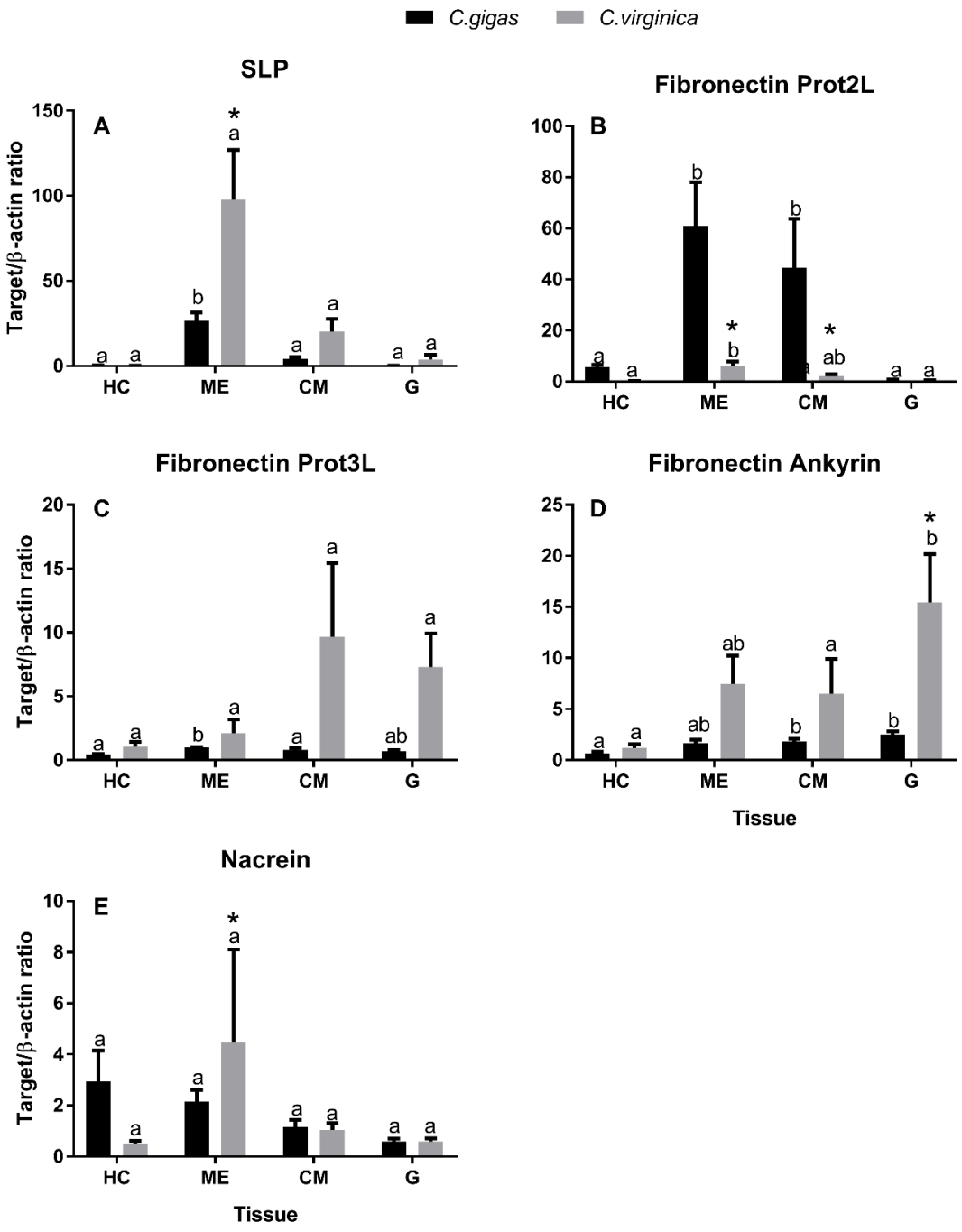

Figure 2. Expression levels of mRNA of genes encoding ECM proteins in tissues of *C. gigas* and *C. virginica*.

Gene names are shown on the figure panes. Dark bars – *C. gigas*, grey bars – *C. virginica*. Different letters indicate the values that are significantly different between different tissues within the same species ($P<0.05$). Asterisks indicate the values that are significantly different between *C. gigas* and *C. virginica* in the same tissue ($P<0.05$).

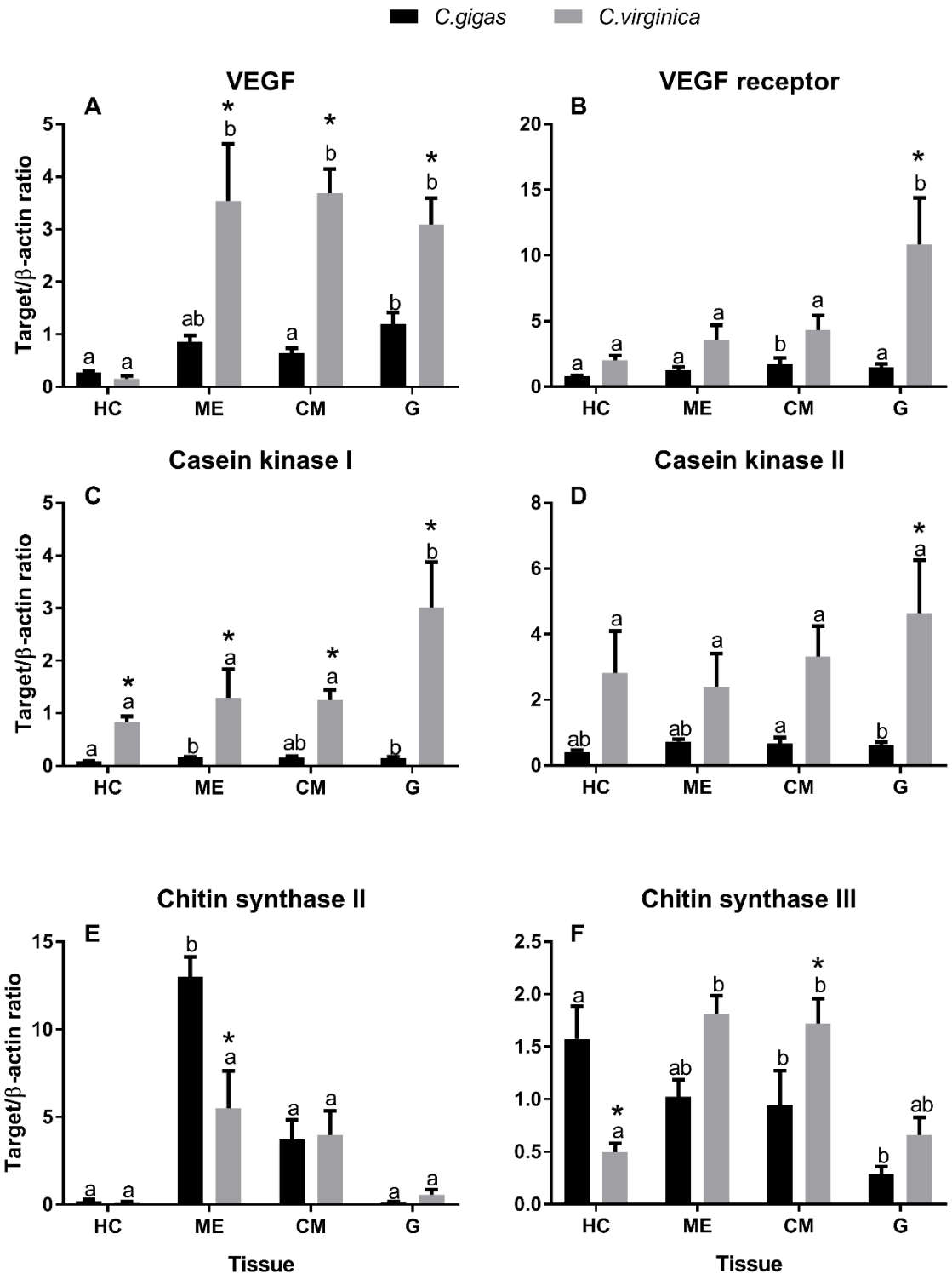

Figure 3. Expression levels of mRNA of genes involved in VEGF pathway and encoding biomineralization-related enzymes in tissues of *C. gigas* and *C. virginica*.

Gene names are shown on the figure panes. Dark bars – *C. gigas*, grey bars – *C. virginica*. Different letters indicate the values that are significantly different between different tissues within the same species ($P<0.05$). Asterisks indicate the values that are significantly different between *C. gigas* and *C. virginica* in the same tissue ($P<0.05$).

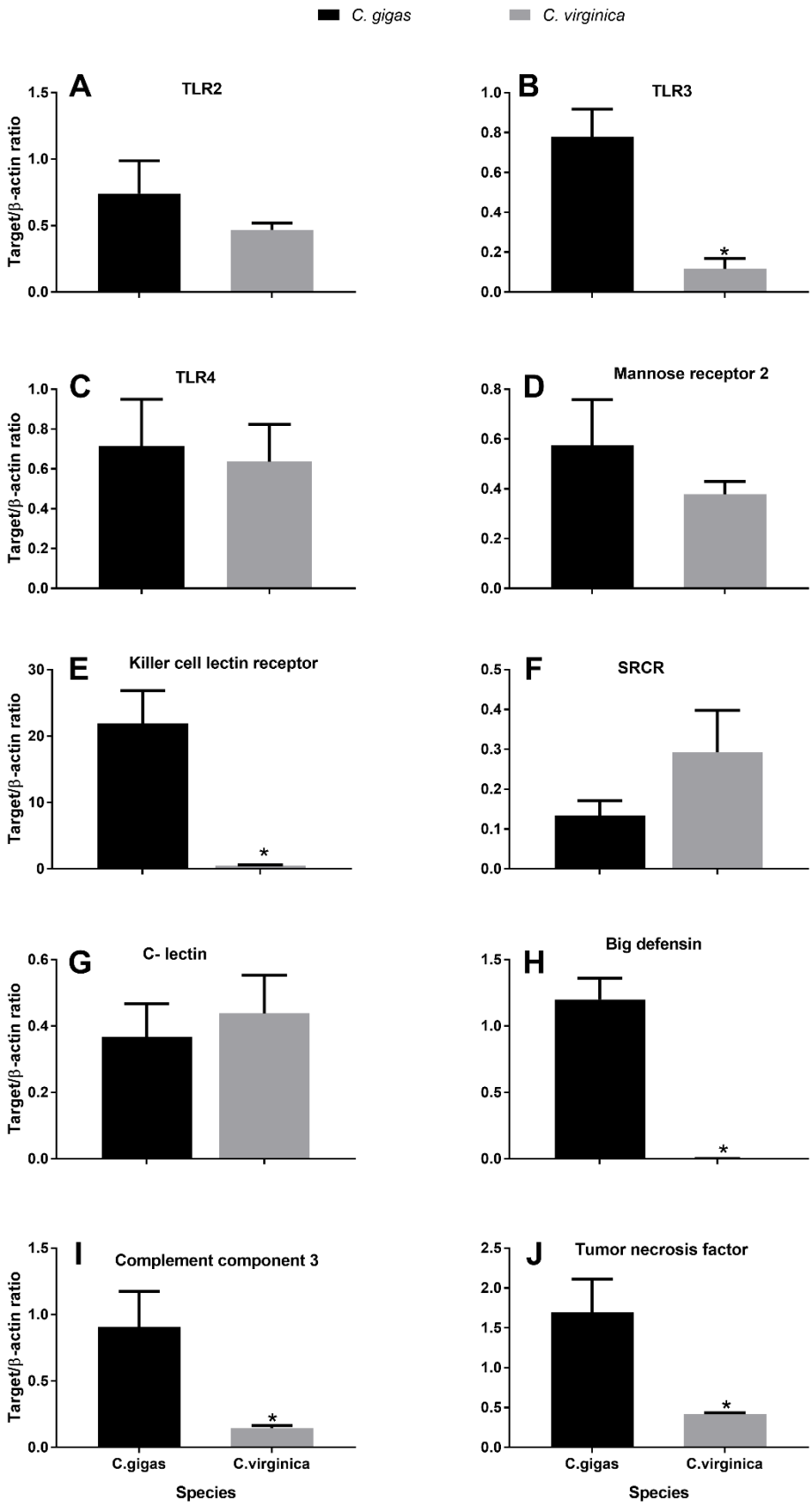

Figure 4. Expression levels of mRNA of immune-related genes in hemocytes of *C. gigas* and *C. virginica*.

Gene names are shown on the figure panes. Dark bars – *C. gigas*, grey bars – *C. virginica*. Asterisks indicate the values that are significantly different between *C. gigas* and *C. virginica* ($P<0.05$).

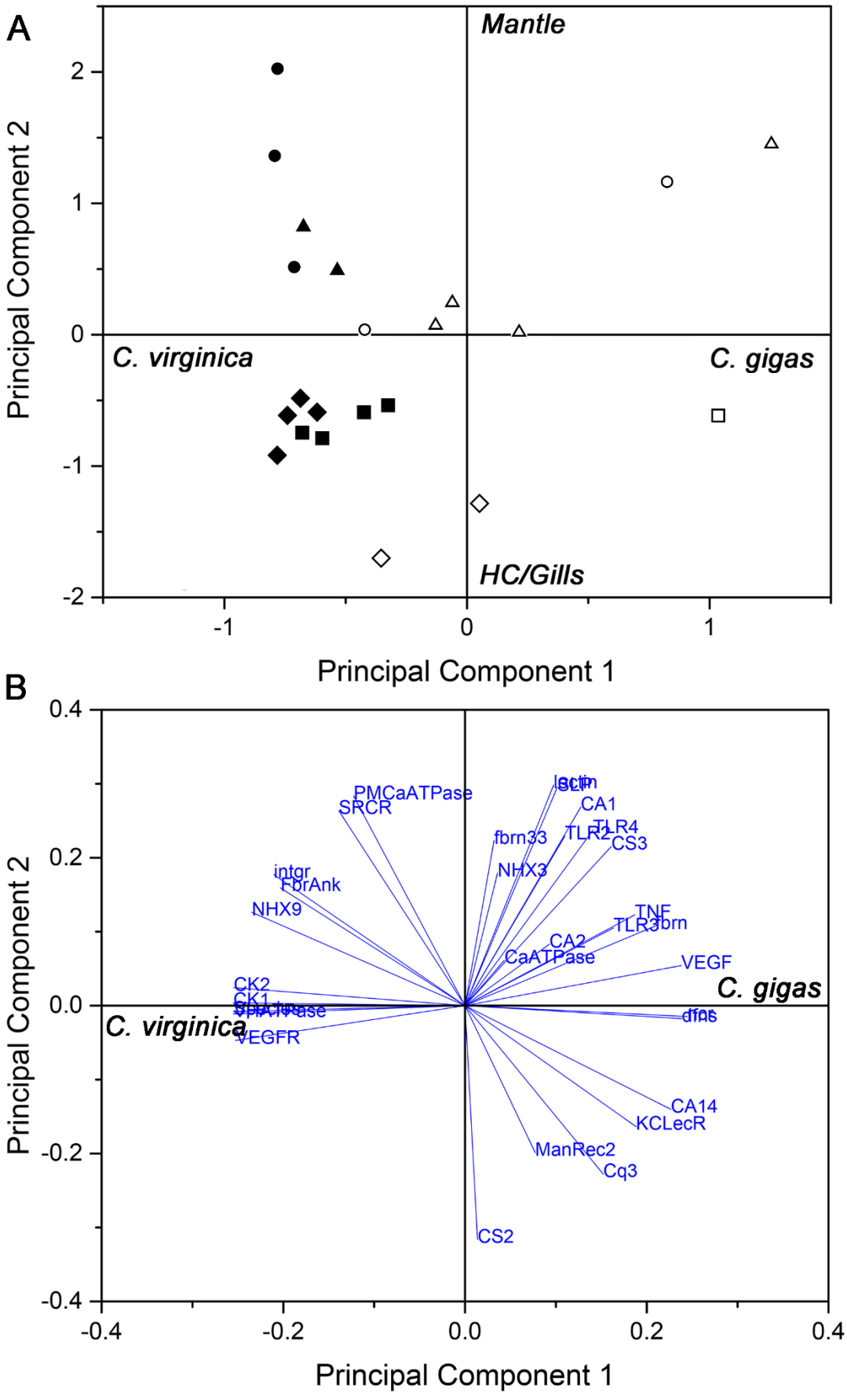

Figure 5. (A) Loading plot showing the results of the PCA analysis of the gene expression patterns of different tissues from *C. gigas* and *C. virginica*. Filled symbols represent tissues of *C. virginica* and empty of *C. gigas*. Diamonds- HCs, squares- Gills, triangles- ME and circles-CM. - Note that factor Species has a strong loading in 1st PC, while factor Tissues has a strong loading in 2nd principal component. **(B)** Loading Loading plot showing the results of the PCA analysis of the gene expression in total HC fraction from the two oyster species studied. Note that the Species factor has a high loading in the 1st principal component, illustrating the point that HC expression patters are different in these two species.

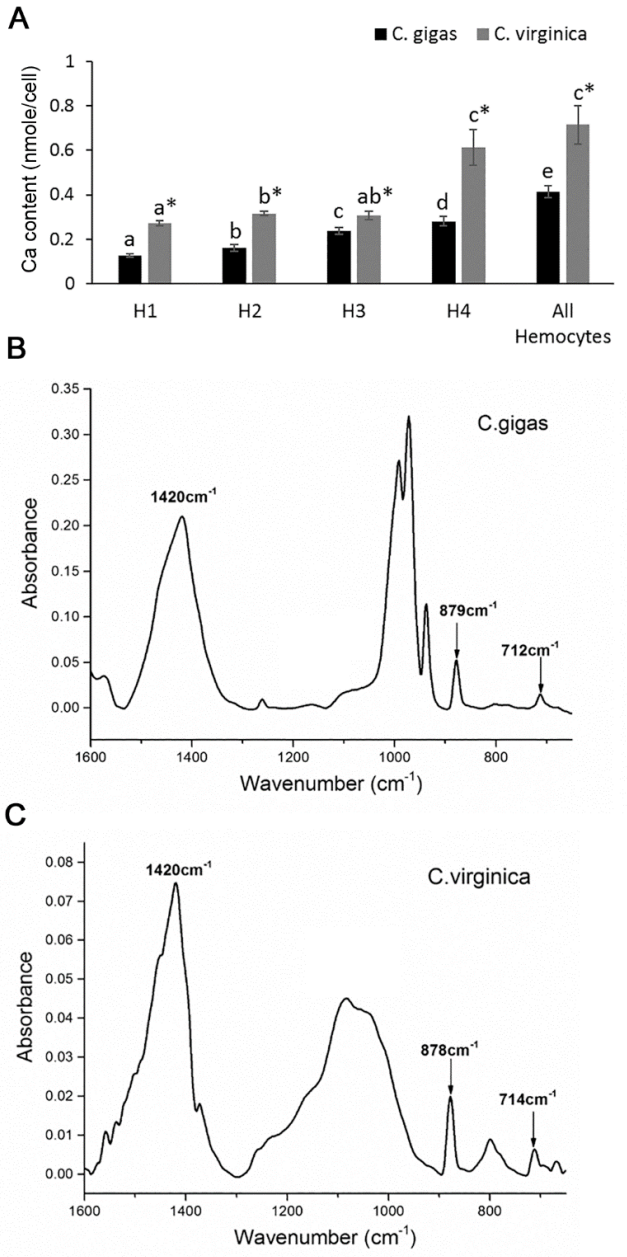

Figure 6. Calcium and mineral analyses of oyster hemocytes.
A - Calcium content in hemocytes of *C. gigas* (black bars) and *C. virginica* (grey bars). Different letters represent statistically significant differences between the hemocyte fractions within a species and asterisks represent statistically significant differences between species within the respective hemocyte fractions. B, C - Typical FTIR spectra of mineral isolated from the total hemocyte fraction of *C. gigas* (B) and *C. virginica* (C). The predominant calcium carbonate phase in these spectra is calcite based on the presence of absorbance peaks at 1422 cm^{-1}, 879 cm^{-1} and 712 cm^{-1}. Note that the other unassigned peaks are due to the impurities.

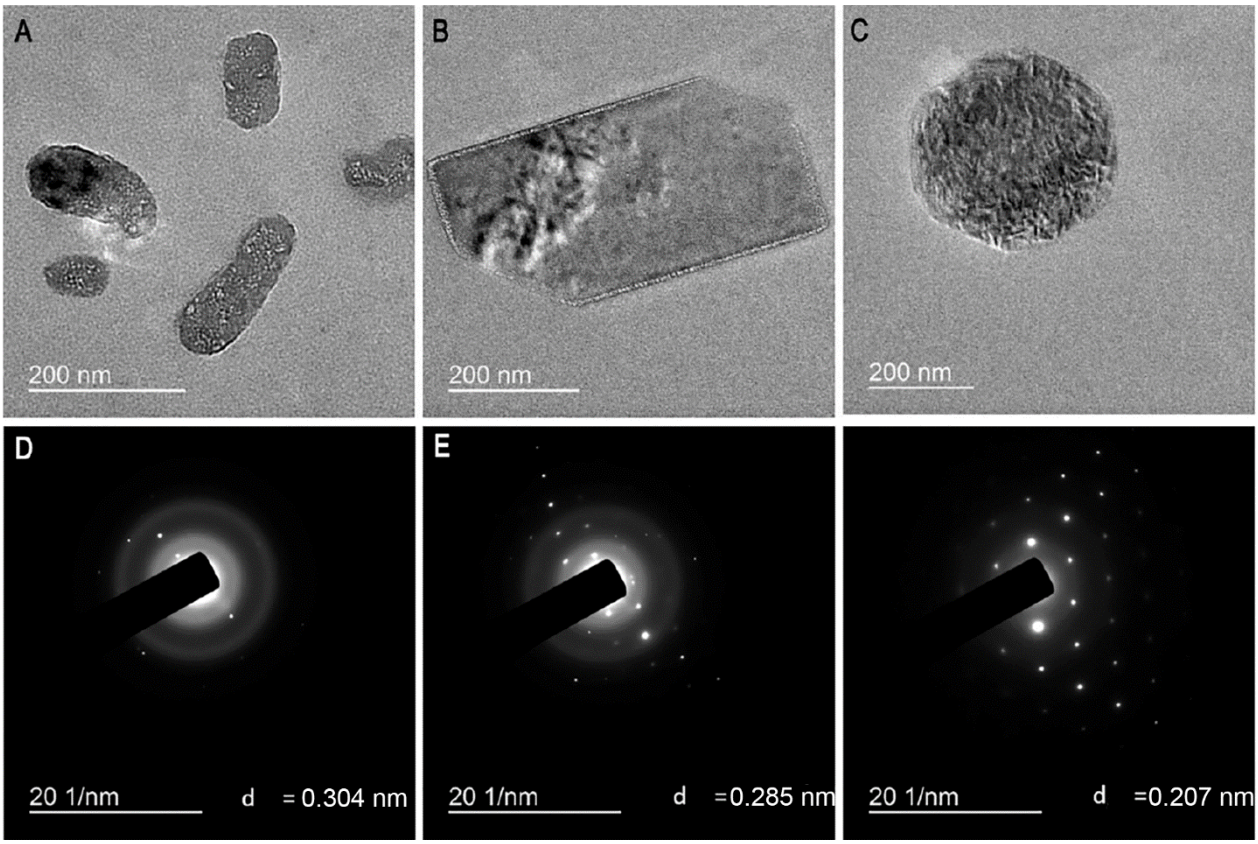

Figure 7. HR TEM micrographs and the diffraction patterns of representative calcium carbonate mineral particles from hemocytes of *C. gigas*.

A, B, C – HR TEM images, D, E, F- the corresponding diffraction patterns. Based on the analysis of the diffraction patterns A represents amorphous calcium carbonate phase transforming into calcite; B is dolomite and C is vaterite. The presence of multiple mineral phases in the sample suggests that the initial calcium carbonate mineral phase in hemocytes is metastable, potentially ACC.

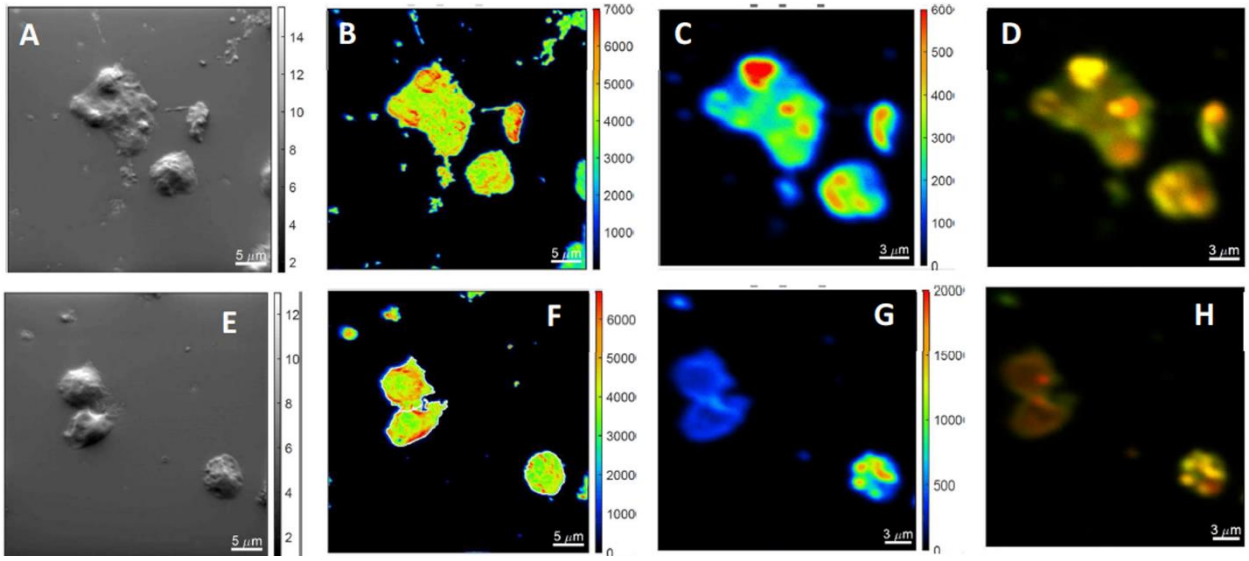

Figure 8. Representative NanoSIMS images showing distribution of Ca and Mg in hemocytes of *C. gigas* and *C. virginica*.

A, B, C, D – *C. gigas*, E, F, G, H – *C. virginica*. A, E – secondary electron images showing general cell morphology, B, F – 12C14N images showing distribution of organic material, C, G – 40Ca+ images; D, H – overlay of 40Ca+ and 24Mg+ signals (red – Ca, green – Mg, yellow – overlap).

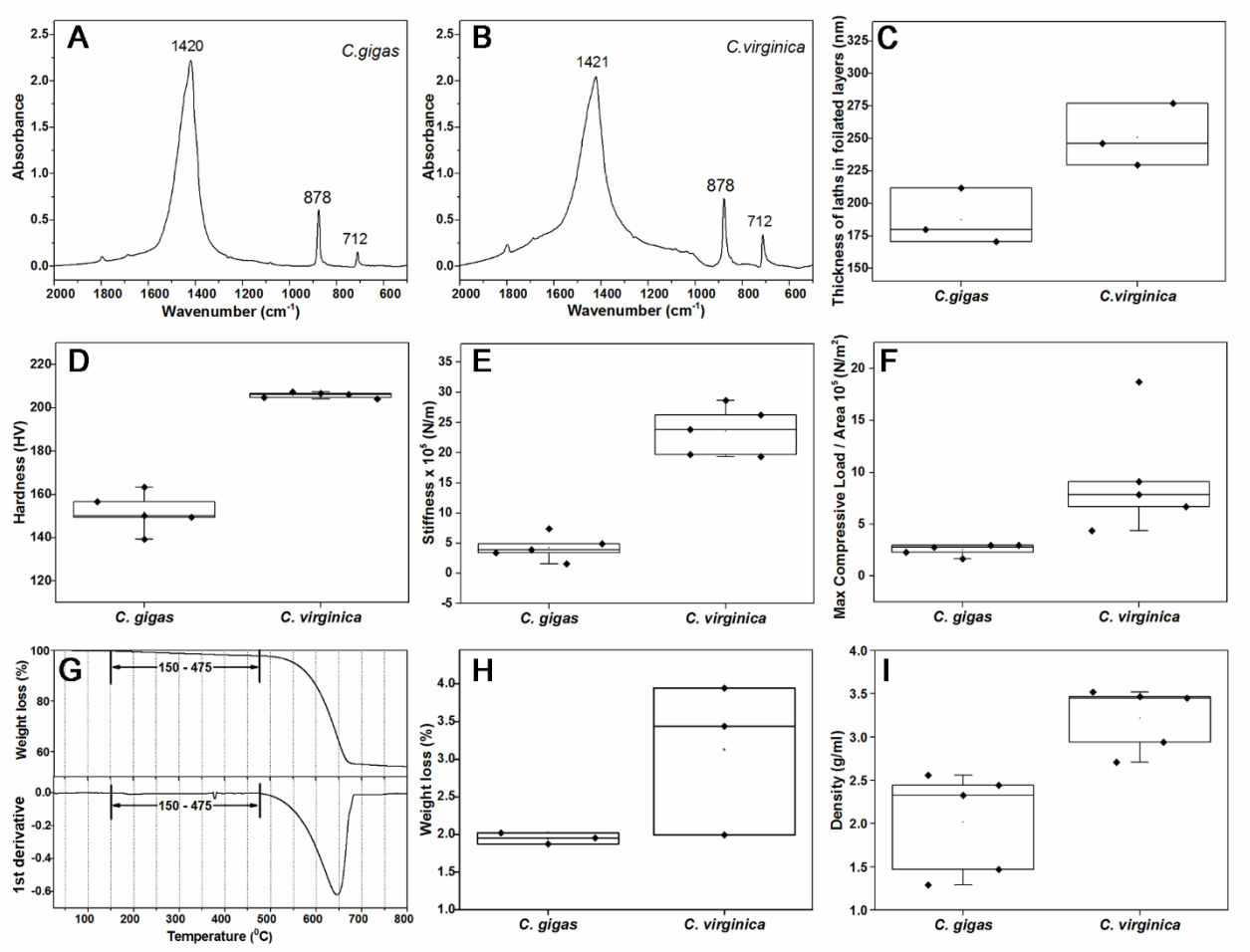

Figure 9. Compositional, structural and mechanical properties of the shells of *C. gigas* and *C. virginica*. **(A,B)** FTIR spectra of shells of *C. gigas* and *C. virginica*. Note the differences in the ν_2/ν_4 (878 cm^{-1}/712 cm^{-1}) intensity ratios. **(C)** Thickness of the individual laths of the foliated layers of the shells. **(D)** Vickers microhardness values of the shells. **(E)** Stiffness of the shells. **(F)** Maximum compressive load of the shells. **(G)** A representative plot showing the results of the TGA, the bottom graph represents the 1nd derivative function of the data. The weight loss in the bracketed region was due to the removal of the shell matrix. Weight loss at the temperatures below 150^{0}C was attributed to water evaporation and above 475^{0}C to $CaCO_3$ thermal decomposition. **(H)** Percentage weight loss values obtained from the TGA. **(I)** Density of the shells acquired using the liquid displacement technique.

Tables

Table 1. ANOVA: Effects of the species and/or tissues (hemocytes, mantle edge, central mantle and gills) on the mRNA expression of biomineralization-related genes of *C. gigas* and *C. virginica*.

F ratios with the degrees of freedom for the effect and the error are given. Significant effects (P<0.05) are highlighted in bold. * - data were normalized using Box-Cox common transformation method.

mRNA expression	Factor effect		
	Species	Tissue	Species x Tissue
CAI	**$F_{1,30}$=12.01 P=0.0035**	**$F_{3,30}$=9.71 P=0.0008**	**$F_{3,30}$=8.66 P=0.0014**
CAII *	$F_{1,30}$=0.45 P=0.509	**$F_{3,30}$=5.80 P=0.004**	**$F_{3,30}$=6.29 P=0.003**
CAXIV	**$F_{1,30}$=11.31 P=0.004**	**$F_{3,30}$=4.56 P=0.018**	**$F_{3,30}$=3.95 P=0.029**
V Type H^+-ATPase	**$F_{1,30}$=12.49 P=0.0030**	**$F_{3,30}$=8.85 P=0.001**	**$F_{3,30}$=8.63 P=0.001**
Ca^{2+}-ATPase	$F_{1,30}$=3.19 P=0.09	**$F_{3,30}$=3.86 P=0.014**	$F_{3,30}$=2.06 P=0.15
PM Ca^{2+}-ATPase *	$F_{1,30}$=0.06 P=0.805	**$F_{3,30}$=53.26 P<0.0001**	**$F_{3,30}$=28.31 P<0.0001**
NHX9	**$F_{1,30}$=24.68 P=0.0002**	**$F_{3,30}$=4.26 P=0.023**	**$F_{3,30}$=4.56 P=0.018**
NHX3*	**$F_{1,30}$=4.79 P=0.039**	**$F_{3,30}$=7.31 P=0.0013**	**$F_{3,30}$=9.82 P=0.0002**
SLP*	$F_{1,30}$=1.16 P=0.29	**$F_{3,30}$=9.87 P=0.0002**	**$F_{3,30}$=3.76 P=0.025**
Fibronectin Prot2L	**$F_{1,30}$=16.87 P=0.0009**	**$F_{3,30}$=5.84 P=0.0075**	**$F_{3,30}$=4.65 P=0.017**
Fibronectin Prot3L*	$F_{1,30}$=0.35 P=0.56	**$F_{3,30}$=13.87 P<0.0001**	**$F_{3,30}$=5.27 P=0.0065**
Fibronectin Ankyrin*	$F_{1,30}$=1.31 P=0.26	**$F_{3,30}$=12.87 P<0.0001**	**$F_{3,30}$=9.25 P=0.0003**
Nacrein-like protein*	**$F_{1,30}$=7.73 P=0.011**	**$F_{3,30}$=9.55 P=0.0003**	$F_{3,30}$=0.97 P=0.42
VEGF*	$F_{1,30}$=0.04 P=0.84	**$F_{3,30}$=5.27 P=0.007**	**$F_{3,30}$=4.34 P=0.015**
VEGF receptor*	**$F_{1,30}$=9.96 P=0.004**	**$F_{3,30}$=9.48 P=0.0003**	**$F_{3,30}$=8.44 P=0.0006**
Casein kinase I	**$F_{1,30}$=63.99 P<0.0001**	**$F_{3,30}$=6.94 P=0.004**	**$F_{3,30}$=6.41 P=0.005**
Casein kinase II	**$F_{1,30}$=10.20 P=0.006**	$F_{3,30}$=0.36 P=0.78	$F_{3,30}$=0.37 P=0.77
Chitin synthase II	$F_{1,30}$=1.48 P=0.24	**$F_{3,30}$=10.84 P=0.0005**	$F_{3,30}$=2.06 P=0.15
Chitin synthase III	$F_{1,30}$=1.21 P=0.29	$F_{3,30}$=2.94 P=0.07	**$F_{3,30}$=6.43 P=0.005**

Table 2. ANOVA: Effects of the species on immune-related traits and ion content of hemocytes of *C. gigas* and *C. virginica*.

F ratios with the degrees of freedom for the effect and the error are given. Significant effects (P<0.05) are highlighted in bold. * - data were normalized using Box-Cox common transformation method.

	Traits	Species Effect
Functional traits	Total HC number	**$F_{1,18}$=5.54 P=0.03**
	Adhesion	$F_{1,18}$=0.01 P=0.91
	Phagocytosis	$F_{1,18}$=1.32 P=0.27
mRNA expression	Integrin*	$F_{1,10}$=4.39 P=0.07
	TLR2	$F_{1,8}$=1.61 P=0.25
	TLR3	**$F_{1,8}$=13.19 P=0.002**
	TLR4	$F_{1,11}$=0.069 P=0.80
	Mannose Rec2	$F_{1,8}$=1.24 P=0.30
	Killer cell lectin like receptor	**$F_{1,8}$=10.14 P=0.02**
	Scavenger receptor cysteine rich*	$F_{1,10}$=1.09 P=0.32
	Tumor necrosis factor	**$F_{1,8}$=7.45 P=0.03**
	Complement component 3	**$F_{1,8}$=7.63 P=0.03**
	C-type lectin	$F_{1,8}$=0.14 P=0.72
	Big defensin	**$F_{1,8}$=34.61 P=0.0006**
Intracellular ion ratios (NanoSIMS)	Ca/Mg ratio	$F_{1,68}$=1.49 P=0.226
	Ca/Na ratio	**$F_{1,68}$=9.14 P<0.001**
	Mg/Na ratio	**F_{168}=45.13 P=0.003**

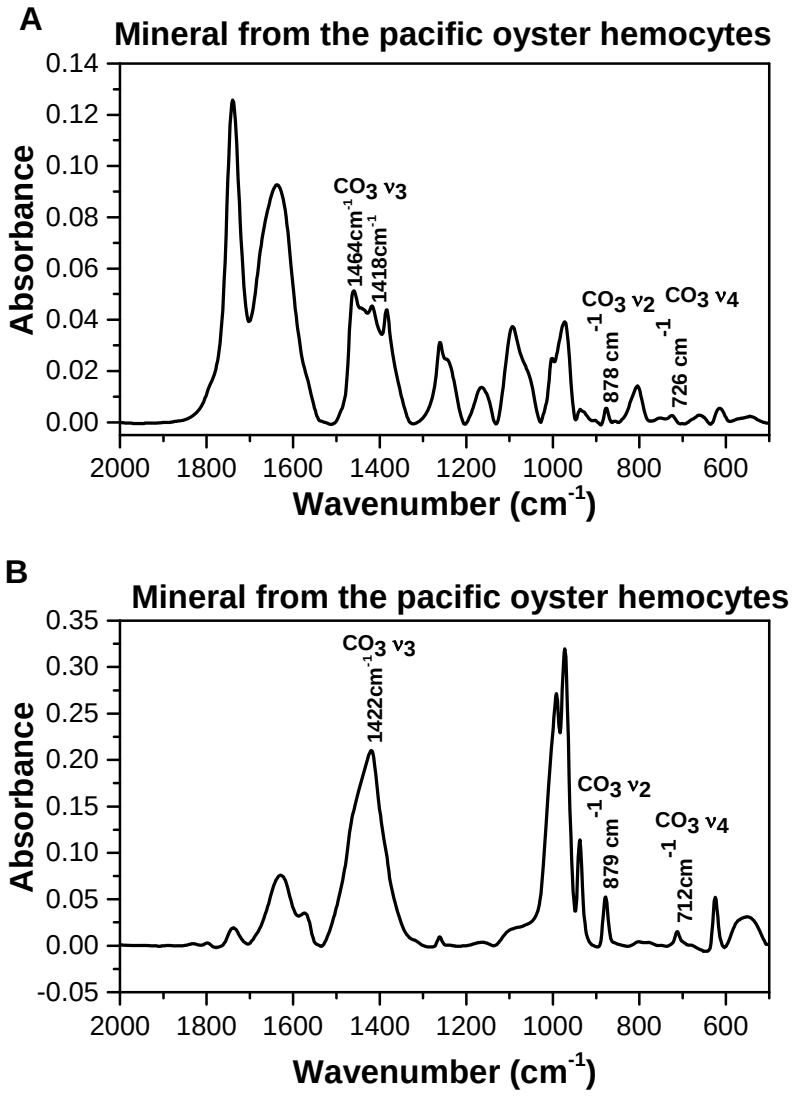

Supplementary Figure 1. Typical spectra of the enriched mineral fractions obtained from the hemocytes of pacific oysters. **A.** The predominant calcium carbonate phase is dolomite based on the presence of absorbance bands at 1464 cm^{-1}, 878 cm^{-1} and 724 cm^{-1}. **B.** The predominant calcium carbonate phase in this spectrum is calcite based on the presence of absorbance peaks at 1422 cm^{-1}, 879 cm^{-1} and 712 cm^{-1}. Note that the other unassigned peaks are due to the impurities. Variations in the calcium carbonate mineral phases in different preparations support the notion that the initial mineral phase is metastable and it transforms into different mineral phases during the preparation.

Supplementary Figure 2. NanoSIMS images of gold-coated samples of hemocytes of *C. gigas*.

A – secondary ion image showing 3D structure of the sample; B - 12C14N signal distribution showing two hemocytes (indicated by arrows); C – 40Ca signal; D – 16 O signal. Note co-localization of the hotspots for Ca and O signals within the hemocytes (panes C and D) indicating presence of calcium carbonate.

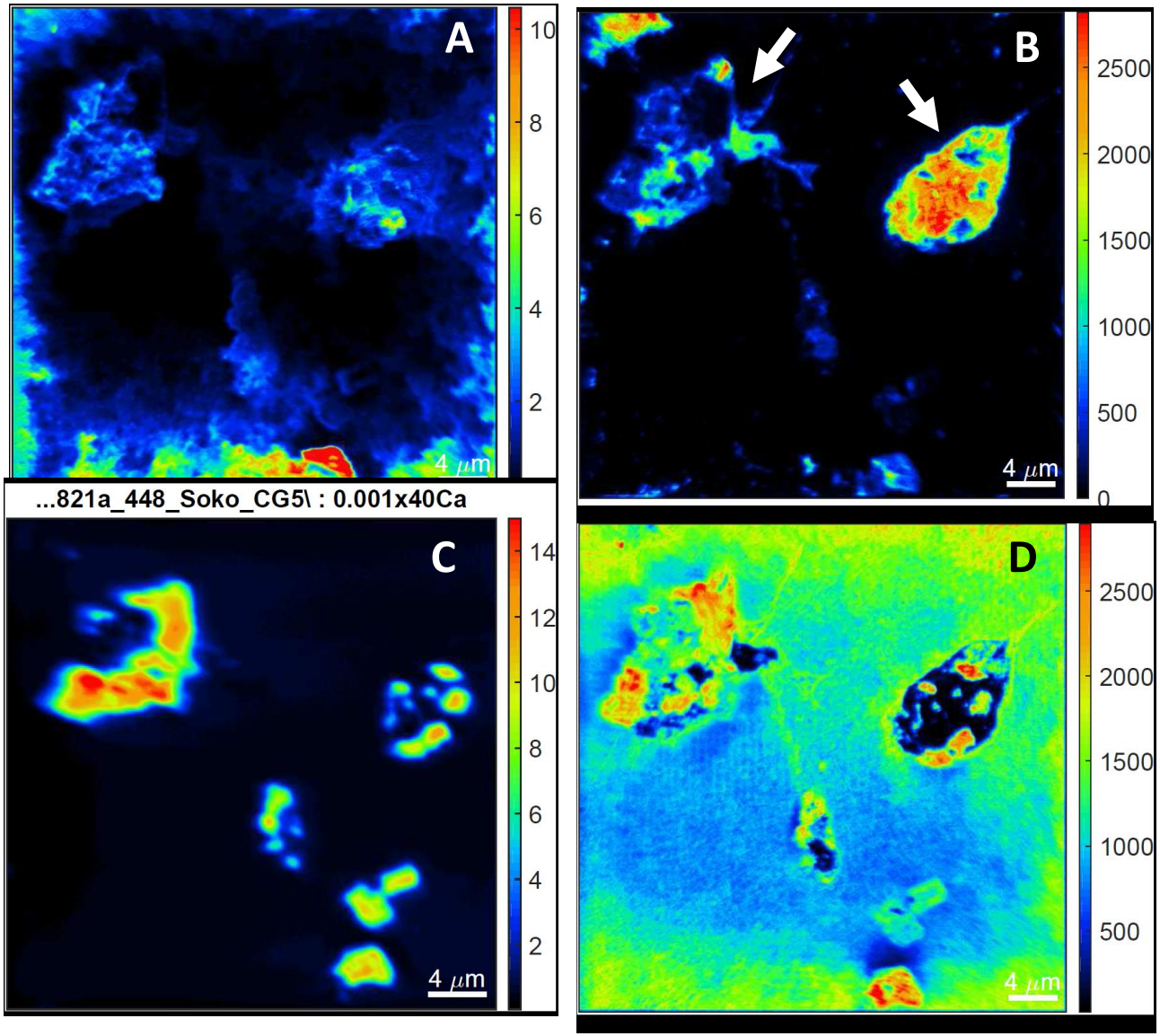

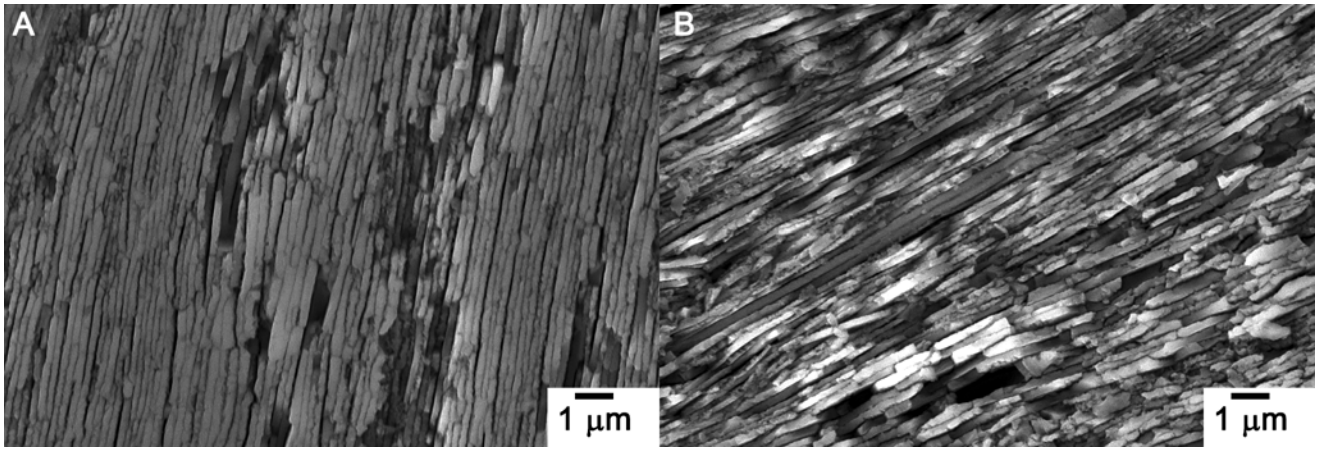

Supplementary Figure 3. SEM micrographs of shell's foliated layer of (**A**) *C. virginica* and (**B**) *C. gigas*

Supplementary Table 1. Primers used to amplify the target biomineralization- and immune-related genes of *C.gigas* and *C. virginica*.

NCBI accession numbers of the sequences used for primer design and annealing temperatures ™ are given for each primer pair.

	Crassostrea gigas			*Crassostrea virginica*		
Target	Accession number	Primer sequence	Tm, (°C)	Accession number	Primer sequence	Tm, (°C)
CAI	XM_011439428.1	FW 5′-AGGGTTGATTCACTCCACATAC-3′	55	XM_011439428	FW 5′-AACCCTTCACCCTCGATCAC-3′	62
		Rev 5′-GCTCCATGGGATAAGAGATTCC-3′			Rev 5′-ACCTCCCACCAAAACATTGGA-3′	
CAII	XM_011449596.1	FW 5′-CATCAACCAGCAGTCAGAAGTA-3′	55	XM_011449596	FW 5′- CTACATGGTCCAGGTCGGTG-3′	60
		Rev 5′-TGTTCCGATCCCTTGTCATTAG-3′			Rev 5′- TTAGCTGTGTCGAAGGGCTC-3′	
CAXIV	XM_011437076.1	FW 5′-AGTGTTCAAGGAGACCATCAAG-3′	55	XM_011437076	FW 5′- AGATGTTCGTTGCTGGTCGG-3′	60
		Rev 5′-CTGTGGTTGAGAGGCTGAATAG-3′			Rev 5′- CAGTGGGTCGGTCCATGTTC-3′	
V-type H^+ ATPase	XM_011420050.1	FW 5′- GCAGTGTCAGCATTGTAGGA-3′	55	XM_011420050	FW 5′- ATCGTACAACTCGTCGGCAA-3′	62
		Rev 5′-GTAGGAGATGAGCCAGTTGATG-3′			Rev 5′- GGGCGTGTATCCATTCTGCT-3′	
Ca^{2+} ATPase	XM_011430632.1	FW 5′- AGGCAAAGGCATCGTCATAG-3′	55	XM_011430632	FW 5′- CAGCAGAGGCAAGCGTTCTA-3′	60
		Rev 5′-GATGAGCCCGATGATACAGAAG-3′			Rev 5′- AGGCCAGCAGCAACAGTATC-3′	
PM Ca^{2+} ATPase	XM_011442008.1	FW 5′- CAACAAGGTCGCCAACAAAG-3′	55	XM_011442008	FW 5′- GGACGAGAGTTCCTTAACGGG-3′	60
		Rev 5′- GGTCAGTTTGCCCTGTAGAA-3′			Rev 5′- TCACCAGCATCTTACCGCTG-3′	
NHX9	762071015_2093292	FW 5′- TGGTGAAGCTGACTGGTATTG-3′	55	762071015_2093292	FW 5′- CTGCTCTTCTGCCTGGTCTT-3′	60
		Rev 5′- CAATGGTTGCCGTCACAAAG-3′			Rev 5′- GTCCCCCAAAAGCCATAGTGA-3′	
NHE3	LOC105349034	FW 5′-GATGATCCAGAGGAGAGCAAAG-3′	55	LOC105349034	FW 5′- CCTGTGTCTGCTGTACAGGTT-3′	60
		Rev 5′-TTGTACGAGGGCTTTCTGTTAG-3′			Rev 5′- CCGCCATAGGCCATGATGAA-3′	
Fibronectin Prot3	XM_011437620.1	FW 5′-CCAGGAGGAAATTTGAGGAGAG-3′	55	XM_011437620	FW 5′- GGGCGAGGTTATGAGACGTT-3′	60
		Rev 5′-GTACTCATAGGGCACTGGTTTAG-3′			Rev 5′- TCCAGCCACATTACAGCAGG-3′	

Fibronectin Prot2	XM_011415803.1	FW 5′- CTCCAGTACACCACAAGTCATC-3′ Rev 5′- AGACACAACTCCGGCAATATC-3′	55	XM_011415803	FW 5′- CGGAATGCAGATGGGTGGAT-3′ Rev 5′- GGGCTGTTGCAACTGATTACC-3′	62
Fibronectin - ankyrin	XM_011451952.1	FW 5′- CTAACAGTGTCCACCACTAAGG-3′ Rev 5′- CCTGTGTCCAGTATCCTCTCTA-3′	55	XM_011451952	FW 5′- TGGGGCAAAGTATGACGACT-3′ Rev 5′- CGTCAGCACCGTCTTTGATG-3′	60
VEGF	XM_011451443.1	FW 5′- CCGGTGCATGTGTACCAATA-3′ Rev 5′- TGATTTCCTCGTCAGTCATTCC-3′	55	XM_011451443	FW 5′- CCACCGCTGATCCTCAACAT-3′ Rev 5′- ACGGAACTGAAGCATGCACT-3′	60
VEGF-R	XM_011457891.1	FW 5′- CGGTCTATGGCTCTGCATAAA-3′ Rev 5′- CAAATGCACCTTGACCCAATAC-3′	55	XM_011457891	FW 5′- CATGTGGGGGTCCTGAAAGC-3′ Rev 5′- ATGCTCCTCTTGGTCCTTTGG-3′	64
Casein kinase I	XM_011448074.1	FW 5′- GGAGGTGGCTGTTAAGTTAGAG-3′ Rev 5′- GCGAGCAGAAGTTGAAGAGA-3′	55	XM_011448074	FW 5′- TGGCAAGGACTTAAAGCCAAC-3′ Rev 5′- ACATGGCAAATTCTGCAGGGA-3′	60
Casein kinase II	XM_011419091.1	FW 5′- CGATGAAGCAGAGATCCCATTA-3′ Rev 5′- CAAACAGCACATGACCAACTAC-3′	55	XM_011419091	FW 5′- AGTGGCAAACGGTGAACGTA-3′ Rev 5′- GTGCCAATAGGCTGATGGGG-3′	60
Chitin synthase II	XM_011425426.1	FW 5′-CGCAACAATGGGCAATAGAG-3′ Rev 5′- CTGATATCGAGGCGGTGAATAG-3′	55	XM_011425426	FW 5′- CCGCCATTTTACACCTTGCC-3′ Rev 5′- CTCGTCGTCGACCCCTAGTA-3′	60
Chitin synthase III	EKC25899	FW 5′-GTACAAATGGGCTCTGGGATAG-3′ Rev 5′-GTCGAACTCACACTGGAAGAA-3′	55	EKC25899	FW 5′-TCAATGCAACAACCAGCAAA-3′ Rev 5′-ATGCGAGTCCCGCAAGATAG-3′	60
Nacrein	NM_001305309.1	FW 5′-CGCCGAGAAGAAACCTCTAAAT-3′ Rev 5′-CCAGAGCCAAACTACGTCTTAC -3′	55	NM_001305309	FW 5′-TTGACGGCAGACATTACCCA-3′ Rev 5′-ACGCCTTTGATTTCTTGACCAT - 3′	60
SLP	AB290411.1	FW 5′- GATCTTCCGTCTTTACGTCCTATC-3′ Rev 5′- AACCGGAGTAAGGTGTTGTATC-3′	55	AB290411	FW 5′-CCAGTACTCGGAACTCGTCG-3′ Rev 5′-AGAACCGCCTGTTCAACGTA-3′	60

Calmodulin	JF508172.1	FW 5′-CCAATGGTGCGAAGCTACTA-3′ Rev 5′-AGGCTGATTTAGACGGTGATG-3′	55	JF508172	FW 5′-TCGGTCGAAGCGAGATCCAT-3′ Rev 5′-TTGATCATGTGTGGCTGCTCT-3′	60
Integrin	XM_011444113.2	FW 5′-GTTTCATGATGCACTGAAGG-3′ Rev 5′-CAATCCTTTTAAGCAACCCG-3′	58	MGID95214	FW 5′-CTGCTCCGATCTGATCAACA-3′ Rev 5′-CATACGTGTCCCCCTGTCTT-3′	55
Killer cell lectin like Rec	XM_011421247.2	FW 5′-AGACGTCTCAAAGGTTCAAA-3′ Rev 5′-TTGATTCTGCCAAACGTAAC-3′	56	BG624932.1	FW 5′-AAAGCCGGTCCTTACTTATGAA-3′ Rev 5′-GCCGGATATGCACCTGTAATA-3′	60
TLR2	EKC29626.1	FW 5′-TCAGGGAACATTGTCACATC-3′ Rev 5′-GTGATAGCCATTCGCAATTC-3′	58	JH819194.1	FW 5′-GCGCTTTATTGACGTTAGAC-3′ Rev 5′-CGTAAACACATGAAACTGGT-3′	58
TLR3	JH816729.1	FW 5′-GTGGGAAGACAGTTCCTAAG-3′ Rev 5′-GCATGTTTGCTATAAAATGCAG-3′	58	MGID92145	FW 5′-TTTGGTTCAAGAACTGGGTT-3′ Rev 5′-GATTAAGGCTCAACAATGGC-3′	58
TLR4	JH817360.1	FW 5′-CAGACGCCGTATATTTGGTA-3′ Rev 5′-TATTTAAGCTCGGGATGTCG-3′	58	MGID89881	FW 5′-GCCTCCGACTGATTGATTTA-3′ Rev 5′-ATACCTCTGAGGATAGGACG-3′	58
Mannose Rec2	XM_011414451.2	Fw GTTCACTTTTACGTTCACCC-3′ Rev 5′-TTTGTTGACATTTTGACGCA-3′	58	XM_011414451.2	Fw GTTCACTTTTACGTTCACCC-3′ Rev 5′-TTTGTTGACATTTTGACGCA-3′	58
SRCR	XM_011436583.2	FW 5′-CCAAATTGCAGATTGAGGTG-3′ Rev 5′-CAGATGCCTTGCTATTTGTG-3′	58	BG624783.1	FW 5′-CACATGCGGCTTCTGTCTAA-3′ Rev 5′-CGGTGATCGTGCTGGTATATG-3′	62
TNF	MGID91531	FW 5′-GCTTTGTAGGGTGTGATTTG-3′ Rev 5′-GTTGTACTTGCCGATGACTT-3′	58	MGID91531	FW 5′-GCTTTGTAGGGTGTGATTTG-3′ Rev 5′-GTTGTACTTGCCGATGACTT-3′	58
complement component 3 (C3)	KF927126.1	FW 5′-GGTATATCCTGTCCAAGCAG-3′ Rev 5′-TGTAGGCAGTCCTTGAGATA-3′	58	KF927126.1	FW 5′-GGTATATCCTGTCCAAGCAG-3′ Rev 5′-TGTAGGCAGTCCTTGAGATA-3′	58
Big defensing	JN251129	FW 5′-TTTGTTGCCTATAGCATCGT-3′ Rev 5′-GTATCTGTAAAGGGCGTAGG-3′	56	CV133156	FW 5′-TGGCAGCTGCTTACGGTATC-3′ Rev 5′-CCCTGTTGTTGGCACAGCTA-3′	60
lectin	XM_011432477.2	FW 5′-TTACAAAACCGTGTCACCTC-3′ Rev 5′-GTATTGCTGTAAAACGCCAA-3′	56	CV088804.1	FW 5′-ATTTGCTCAGCCTTGAATGG-3′ Rev 5′-GTCCCTCCCACCCAGTAGTT-3′	55
β-actin	X75894	FW 5′-TTGGACTTCGAGCAGGAGATGGC-3′ Rev 5′-ACATGGCCTCTGGGCACCTGA -3′	55	X75894	FW 5′-CAC AGC CGC TTC CTC ATC CTC C-3′ Rev 5′-CCG GCG GAT TCC ATA CCA AGG-3′	55

Supplementary Table 2. Principal Component Analysis (PCA) of biomineralization-related genes in oysters.

Tissues were encoded as follows: 1- central mantle; 2- outer mantle edge; 3 - gills; 4 - hemocytes. Species were encoded as follows: 1 – *C. gigas*, 2 – *C. virginica*. CK – creatine kinase, CS – chitine synthase, CA – carbonic anhydrase, SLP - silk-like protein, VEGF - vascular endothelial growth factor, VEGF-R - vascular endothelial growth factor receptor, FN – fibronectin, FNAnk – fibronectin-ankyrin, NHX – sodium-proton exchanger, PM Ca2+ ATPase – plasma membrane Ca2+ ATPase.

PC	Eigenvalue	Percentage of Variance	Cumulative
1	8,61749	41,04%	41,04%
2	3,11565	14,84%	55,87%
3	2,04403	9,73%	65,61%
4	1,29895	6,19%	71,79%
5	1,06344	5,06%	76,86%
6	0,88823	4,23%	81,08%
7	0,83594	3,98%	85,07%
8	0,70519	3,36%	88,42%
9	0,53363	2,54%	90,96%
10	0,41985	2,00%	92,96%

Loadings

	PC1	PC2	PC3	PC4	PC5
species	0,21015	-0,11856	-0,32863	0,25598	0,02771
tissue	-0,02365	-0,42799	0,04893	0,06324	-0,17433
CK1	0,32375	-0,00357	0,01581	-0,02708	-0,09451
CK2	0,28498	0,0085	-0,03804	0,07719	-0,01627
CS2	-9,63E-04	0,46203	0,04119	0,22952	-0,01764
CS3	0,04843	0,2463	-0,42081	-0,15509	0,07272
CA1	0,26141	-0,08978	0,18878	-0,15123	-0,32732

CA2	0,18612	0,08529	0,14074	-0,22947	0,28101
CA14	-0,10233	0,35441	0,35062	0,01579	1,92E-04
VEGF	0,24633	0,20806	-0,24224	0,00434	-0,26342
VEGF-R	0,29119	-0,01567	0,11634	-0,11517	-0,27843
SLP	0,07634	0,31619	-0,30643	0,35547	-0,28692
NHX3	0,30943	-0,07496	0,18799	-0,18957	-0,06524
NHX9	0,33004	-0,01972	0,09116	-0,07965	-0,02703
Ca2+ ATPase	0,23366	0,16476	0,187	-0,11612	0,2614
PM Ca2+ ATPase	0,23663	-0,06606	-0,16949	0,13106	0,42184
V H+ ATPse	0,09481	-0,26131	0,20689	0,52937	0,2529
Nacrein	-0,05897	0,0293	-0,26578	-0,51107	0,20816
FN3-2	-0,10338	0,35034	0,37273	0,07524	0,0142
FN3-3	0,26524	0,11025	-0,01402	0,0975	0,41358
FNAnk	0,3056	0,05037	0,06871	0,04597	-0,09432

Supplementary Table 3. Pearson correlation analysis of mRNA levels of biomineralization-related genes in oysters.
Tissues were encoded as follows: 1- central mantle; 2- outer mantle edge; 3 - gills; 4 - hemocytes. Species were encoded as follows: 1 – C. gigas, 2 – C. virginica. CK – creatine kinase, CS – chitine synthase, CA – carbonic anhydrase, SLP - silk-like protein, VEGF - vascular endothelial growth factor, VEGF-R - vascular endothelial growth factor receptor, FN – fibronectin, FNAnk – fibronectin-ankyrin, NHX – sodium-proton exchanger, PM Ca2+ ATPase – plasma membrane Ca2+ ATPase.

Click here to Download Table S3

Supplementary Table 4. Principal Component Analysis (PCA) of the transcriptomic profiles of oyster hemocytes.

Species: 1 - *C. gigas*, 2 - *C. virginica*. CK – creatine kinase, CS – chitin synthase, CA – carbonic anhydrase, SLP - silk-like protein, VEGF - vascular endothelial growth factor, VEGF-R - vascular endothelial growth factor receptor, FN – fibronectin, FNAnk – fibronectin-ankyrin, NHX – sodium-proton exchanger, PM, Cq3 - complement component 3, SRCR - scavenger receptor cysteine rich, TNF - tumor necrosis factor.

PC	Eigenvalue	Percentage of Variance	Cumulative
1	13,63	43,96%	43,96%
2	6,83	22,05%	66,01%
3	5,71	18,41%	84,42%
4	3,11	10,05%	94,47%
5	1,72	5,53%	100,00%

	PC1	PC2	PC3	PC4	PC5
Species	**0,261**	-0,100	0,009	0,007	0,012
lectin	0,095	**0,245**	**0,260**	-0,027	0,211
SRCR	-0,087	**0,294**	-0,222	-0,056	-0,097
KC lectin like Rec	0,156	**-0,248**	-0,108	0,233	0,087
integrin	-0,116	**0,268**	0,010	-0,087	**-0,421**
defensin	0,228	-0,121	-0,134	-0,150	0,103
TNF	0,211	0,016	0,188	-0,232	-0,105
Mannose Rec2	0,062	**-0,262**	0,016	**0,392**	-0,026
Cq3	0,121	**-0,310**	-0,058	-0,195	0,065
TLR2	0,158	0,184	-0,184	**-0,268**	0,084
TLR4	0,141	0,193	-0,221	-0,168	**0,249**
TLR3	0,200	0,008	-0,179	**-0,293**	-0,031
CK1	**0,260**	0,031	-0,010	0,081	-0,174
CK2	0,138	0,128	**0,331**	0,022	0,002
CS2	0,106	**-0,288**	0,203	-0,108	-0,064
CS3	0,224	0,164	0,028	0,197	0,068
CA1	0,219	0,185	-0,108	0,109	0,053
CA2	0,219	0,070	0,133	-0,260	0,037
CA14	0,108	**-0,281**	-0,192	-0,131	0,147
VEGF	-0,171	0,103	-0,094	0,195	**0,458**
VEGFR	0,019	0,002	**0,349**	0,017	**0,416**
SLP	0,237	0,115	-0,151	0,048	0,073
NHX3	0,225	0,034	0,166	0,206	-0,091
NHX9	0,216	0,227	0,018	-0,043	0,039
Ca2+ATPase	0,189	-0,179	-0,186	0,153	0,118
PM Ca ATPase	**0,254**	0,129	0,012	0,041	0,046
V H+ ATPAse	-0,204	0,160	0,088	0,005	**0,354**
SLP	0,011	0,016	**0,417**	-0,037	0,029
FN3-2	0,143	0,168	-0,016	**0,375**	-0,228
FN3-3	0,169	-0,143	**0,277**	-0,089	-0,081
FNAnk	0,219	0,124	-0,081	0,256	0,029

Supplementary Table 5. Pearson correaltion analysis of the transcriptomic profiles of oyster hemocytes.
Species: 1 - *C. gigas*, 2 - *C. virginica*. CK – creatine kinase, CS – chitin synthase, CA – carbonic anhydrase, SLP - silk-like protein, VEGF - vascular endothelial growth factor, VEGF-R - vascular endothelial growth factor receptor, FN – fibronectin, FNAnk – fibronectin-ankyrin, NHX – sodium-proton exchanger, PM, Cq3 - complement component 3, SRCR - scavenger receptor cysteine rich, TNF - tumor necrosis factor.

Click here to Download Table S5